



Using a Building as Thermal Storage and Model Predictive Control of a Heat Pump for Grid Stabilization

Master's thesis of

Vivien Geenen

at the Department of Mechanical Engineering
Institute for Automation and Applied Informatics (IAI)

Reviewer: Prof. Dr. Veit Hagenmeyer
Second reviewer: apl. Prof. Dr. Jörg Matthes
Advisor: Moritz Frahm, M.Sc. and Frederik Zahn, M.Sc.

14. June – 14. December 2021

I declare that I have developed and written the enclosed thesis completely by myself, and have not used sources or means without declaration in the text.

PLACE, DATE

.....

(Vivien Geenen)

Kurzfassung

Abstract

Contents

Kurzfassung	i
Abstract	ii
1 Introduction	1
1.1 Objective of this work	2
1.2 Related work	2
1.3 Content structuring	4
2 Foundations	5
2.1 Thermal basics	5
2.1.1 Balancing energy	5
2.1.2 Conduction	6
2.1.3 Convection	7
2.1.4 Radiation	7
2.2 Lumped capacitance model	8
2.2.1 Electrical analogy	8
2.3 Model predictive control (MPC)	10
2.3.1 Cost function	12
2.3.2 Dynamics	12
2.3.3 Constraints	13
2.4 The reference building	13
3 Modelling	15
3.1 The modelling strategies	15
3.2 The water reservoir model	17
3.3 The building model	18

Contents

3.3.1	Parameter identification	21
3.3.2	Training and verification of the thermal model	22
3.4	The state-space formulation	24
4	Experiments	26
4.1	Experiment 1	26
4.1.1	Data of the experiment 1	27
4.2	Experiment 2	28
4.2.1	Data of the experiment 2	29
4.3	Findings of the experiments	30
5	Model predictive control	32
5.1	Framework conditions of the MPC	32
5.1.1	Characteristic diagram of the heat pump	32
5.1.2	Occupancy schedule	33
5.1.3	Past data	34
5.2	The Constraints	35
5.2.1	Constraints of the control signals	35
5.2.2	Constraint of output	35
5.2.3	Constraints of the states	36
5.2.4	Integration method and its constraint	36
5.3	The Cost function	37
5.4	Workflow of the MPC script	38
5.5	Choice of weightings and horizon	39
5.5.1	Average comfort and grid services over the weightings	40
5.5.2	Choice of the horizon	42
6	Results	44
7	Conclusion	45
8	Outlook	46
	Bibliography	47
A	Appendix	54

A.1	Model values	54
A.2	Matrices of state-space formulation	54
A.3	Laboratory journal	57
A.4	Average comfort and grid services	59

List of Figures

2.1	Sample of a wall with thermal resistances	9
2.2	Sample RC- network	9
2.3	MPC structure of the control loop	11
2.4	Construction plan of the building [37]	14
3.1	Figure of the water reservoir with the heat flows	17
3.2	Structure of the thermal model in RC- analogy	21
3.3	Workflow of grey-box modelling with Matlab	21
3.4	Training of the building model	23
3.5	Verification of the building model	24
3.6	RMSE and R_{\max} of the output for training and verification period	24
4.1	Electrical consumption of the building and air temperature inside the rooms during the experiment 1	28
4.2	Electrical consumption of the building and air temperature inside the rooms during the experiment 2	30
5.1	Interpolation of the characteristic diagram of the heat pump with nominal power according to [42]	33
5.2	Occupancy schedule of the reference building	33
5.3	Dynamic price of electricity [56] and shifted dynamic price of electricity	34
5.4	Workflow of the MPC script	39
5.5	AC and GS for $N = 24h$	41
5.6	Measured data of the reference building: T_{inside} over three days	42
5.7	Curve of the sum of cost over simulation time for different N	43

A.1	AC and GS for $N = 12h$	59
A.2	AC and GS for $N = 18h$	59
A.3	AC and GS for $N = 30h$	60

List of Tables

2.1	dimensions of the matrices	12
3.1	Advantages and disadvantages of grey-box modelling	16
3.2	Advantages and disadvantages of white-box modelling	16
3.3	Explanation of the special material and state dependant values of the differential equation of the inside temperature	19
3.4	Explanation of the special material and state dependant values of the differential equation of the envelope temperature	20
3.5	Conclusion of relevant information about the grey-box model	23
4.1	Technical data and configuration during the experiments [53], [54], [55]	27
5.1	Weighting factor	38
5.2	AC for different N	41
5.3	GS for different N	41
A.1	Start and identified values of the model parameters	54
A.2	Laboratory journal: 16. July - 18. July 2021	57
A.3	Laboratory journal: 26. July - 1. August 2021	58

1. Introduction

Climate change is challenging the entire world. In the Paris Agreement, the United Nations (UN) agrees to keep the rise in global average temperature significant under two degrees Celsius [1]. To achieve this aim every nation has to reduce its greenhouse gas emissions. This calls for changes in the mobility sector, industry, and energy production, for example. Germany intends to implement this by promoting electromobility, using hydrogen in industry, and energy transition [2]. In particular, the energy transition that has already been initiated has to be driven forward. That means the expansion of renewable energies and decreasing conventional power plants. The German government is aiming to phase out coal-fired power plants by 2038 [3]. For covering the energy demand, a high increase in photovoltaics and wind power is necessary in a few years.

Unfortunately, a disadvantage of this renewable energy is that they fluctuate with the weather and do not release energy by demand. In addition, more renewable energies lead to more intense instabilities in the grid. In the first solution approach, energy storage and demand side management (DSM) are used to implement the stable grid in the future. Batteries, pumped hydroelectric energy storage, thermal energy storage, and much more could store an excess of power during a sunny or windy day. Furthermore, DSM can shift loads to stabilize the grid. Load shifting is part of DSM [4] and already used industrially. Another approach is to use residential buildings as thermal storage and demand response to contribute to grid stability [5]. As a promising DSM technology, the control of heating, ventilation, and air conditioning (HVAC) systems could be used. Particularly controlling heat pumps of buildings seem auspicious. As at least 1.25 million heat pumps are already installed in Germany, and the tendency is increasing [6].

The implementation of this approach needs a control strategy ensuring consumer comfort also during changing weather conditions. Model predictive control (MPC) is one suitable instrument to integrate forecasts of weather and control heat pumps in buildings for stabilizing the grid with the thermal storage of the building. Research has already shown the possibilities of MPC to shift loads, to save energy and costs [7], [8], [9]. On the other hand, researchers

1. Introduction

investigate the impact of occupancy plans on energy consumption in buildings. They prove a significant energy-saving potential [10]. This thesis picks up the advantages of an occupancy plan, and it analyses consumption, comfort, and grid service of an MPC with and without an occupancy plan of the building.

1.1. Objective of this work

This thesis aims to design a control system, which simultaneously serves the grid and comply with the required comfortable internal temperature range, for the heat pump of a building in the so-called "Living Lab" of the Karlsruhe Institute of Technology (KIT) at Campus North. The implementation is to be carried out using the control method Model Predictive Control. This method enables to predict the future thermal behaviour of the building and to react to the actual and future fluctuations of the weather or the grid for example. In the first step, a thermal model of the building behaviour must be created. For this purpose, the physical structure of the model is to be determined. Appropriate assumptions can be made to reduce the complexity of the thermal behaviour of the building. Furthermore, the resulting model should apply parameter identification from measurements to obtain a grey-box model, i.e., a combination of physical model structure and optimisation with measurement data. After the verification of the thermal model using measured data from the Energy Lab 2.0 from the KIT, an optimal control problem shall be created. The aim is to construct an MPC algorithm and to simulate its application. The software used will be Matlab/Simulink.

1.2. Related work

Extant literature investigates thermal modelling and controlling of buildings. Kramer et al. [11] summarize in a literature review thermal modelling approaches such as white-box, grey-box, and black-box models and present how researchers apply these approaches. After this review, further authors identify their thermal model parameters with measurements and use the grey-box modelling approach [12], [13], [14]. Coakley et al. [15] see the advantages of grey-box modelling in the short development time for the model, fidelity of predictions, and the interaction of building, system and environmental parameters. One disadvantage is that modellers need a high level of knowledge in physical and statistical modelling [15]. Furthermore, Cigler et al. [16] and Hazyuk et al. [8] see the advantages of grey-box models

1. Introduction

and work with them in their MPC applications for thermal management in buildings. Regardless of the type of model, MPC is utilised for control of heating, ventilation, and air conditioning (HVAC) systems in buildings for a variety of reasons. Researchers are interested in the reduction of energy consumption [8] and saving costs [9] while obtaining thermal comfort. Oldewurtel et al. [7] present how to decrease or shift the peak load of buildings. On the other hand, the following two articles refer to the potential of heat pumps for grid services. Among others, the report "Wärmepumpen in Bestandsgebäuden" examines the load shifting potential of grouped heat pumps. The researchers determine 4 to 14 GWh load shifting potential for one million heat pumps [17]. Kohlhepp and Hagenmeyer [5] introduce a method to assess the technical potential of HVAC systems for grid services. Especially, they analyse for heat pumps 5.2 TWh electrical demand in Germany per year. The researchers apply the above topics grey-box modelling and MPC for heat pumps to the realization of grid services, e.g. by DSM. Avci et al. [18] give an early indication of the potential of grid services using real-time pricing. For application of DSM, most researches apply a dynamic price signal, although their focus differs e.g. according to the type of buildings [19], [20] or the type of optimisation [19], [21]. Another interesting part of research is the energy saving potential by planning the occupancy of buildings. Wang et al. [10] show in their paper that 13 percent of energy can be saved by occupancy-based controls for an office building. Liang et al. [22] investigate an occupancy schedule with for example machine learning approaches to better control of HVAC systems and consequently to save energy.

This thesis applies occupancy schedules into the MPC formulation to investigate the potential of included occupancy behaviour on control metrics. A simple occupancy plan should be used to examine whether comfort, grid services, and energy consumption can be improved compared to an MPC without an occupancy plan. Consequently, in this thesis, an MPC is created with a grey-box model and grid services are implemented with real-time pricing, similar to the papers above. But herein, the potential of an occupants schedule is analysed at a real reference building during focusing on the aim of grid services. This thesis finds an answer to the question: How is the difference between an MPC with and without occupants schedule concerning grid services, energy consumption and comfort?

1.3. Content structuring

Strukturierung meiner Thesis erläutern

2. Foundations

This work is based on foundations, which are summarized in this chapter. This includes thermal basics, foundations about thermal modelling, and model predictive control (MPC).

2.1. Thermal basics

2.1.1. Balancing energy

It is necessary to comprehend the basics of thermodynamics to understand the structure of a thermal model. The first law of thermodynamics is the general energy balance and is formulated for unsteady and open systems as follows [23]:

$$\sum_i \dot{Q}_i + \sum_j \dot{W}_j + \sum_k \dot{m}_k \cdot \left(h + \frac{c^2}{2} + gz \right)_k = \frac{d}{dt} \sum_l U_l \quad (2.1)$$

In terms of a building, we set the work \dot{W} to zero according to the relationship $W = \int P dt - \int p dV$ [23] because a building can't change the volume V , and we have no additional mechanical power P . If we have no mass flow \dot{m} in our system, we obtain a closed system. Regarding buildings, mass flows could be airflow through the window, for example. Then we also consider the enthalpy h , the fluid velocity c , the high z and the gravitational acceleration g .

Since we do not consider airflow, we use the closed system with the heat flows \dot{Q}_i and the inner energy U_l .

$$\sum_i \dot{Q}_i = \frac{d}{dt} \sum_l U_l \quad (2.2)$$

2. Foundations

The deduction of the inner energy U starts with the complete differential description of the specific inner energy du as [23]:

$$du = \left(\frac{\partial u}{\partial T}\right)_v dT + \left(\frac{\partial u}{\partial v}\right)_T dv \quad (2.3)$$

The specific volume dv is negligible in buildings, and the specific heat capacity during constant volume has the expression $c_v = \left(\frac{\partial u}{\partial T}\right)_v$ [23]. After replacing the specific values by volume, we obtain the relation for the inner energy U , with the mass m .

$$dU = mc_v dT \quad (2.4)$$

It applies to substances with a specific volume regardless of the pressure that $c_v = c_p = c$.

We account for different heat flows and for the inner energy in the energy balance in Equation 2.1. However, there are three mechanisms of heat transfer, which are explained in the following sections: Heat conduction, heat convection, and heat radiation [24]. Thermal modelling of buildings requires all of these mechanisms. For example, conduction is the primary part of heat transfer through walls or floors. Convection occurs on the inside and the outside of the building between the walls and the air. To integrated the impact of the sun, radiation is needed, for example.

2.1.2. Conduction

Conduction means that heat energy is directed in a solid or fluid. Molecules within the solid or fluid have higher energy when the temperature is higher. They transfer the energy to neighbouring molecules with smaller energy. Without a heat source, the temperature difference between a hot and a cold location of the molecules decreases.[25]

The equation

$$\dot{\mathbf{q}} = -\lambda \nabla T \quad (2.5)$$

describes the conduction according to Fourier [24]. λ is the thermal conductivity with the assumption of being constant and $\dot{\mathbf{q}}$ and T represent the specific heat flux and the temperature. The thermal conductivity is dependent on the material, such as concrete, wood or bricks. To know the heat flux \dot{Q} , it is necessary to expand the above equation with the area A ,

2. Foundations

the thickness of the conductive medium d and a temperature difference ΔT assuming one significant direction of the heat flux \dot{Q} to:

$$\dot{Q} = \frac{A\lambda}{d}\Delta T \quad (2.6)$$

In terms of buildings, the conductive medium could be walls, floors or roofs.

2.1.3. Convection

Macroscopic movements of a fluid lead to the transport of kinetic energy and enthalpy. This mechanism is called convection. These movements are generated by external forces or by internal forces like balancing the pressure or temperature [24].

Newton's law of cooling describes the convective heat transfer \dot{Q} as

$$\dot{Q} = \alpha A(T_w - T_\infty) \quad (2.7)$$

with the heat transfer coefficient α , especially for building modelling the wall temperature T_w and the environment temperature T_∞ [26]. There are two possibilities to determine the heat transfer coefficient. Both require a temperature difference ΔT and either a temperature gradient $\partial T/\partial x$ or a heat flux \dot{Q} . [24]

2.1.4. Radiation

Every body emits heat radiation to the environment with electromagnetic waves. Heat radiation does not need matter for energy transportation. As shown in the following equation, the temperature T of the body influences heat radiation.[24]

$$\dot{q} = \sigma T^4 \quad (2.8)$$

This correlation applies to a black body, where \dot{q} is a heat flux and σ represents the Stefan-Boltzmann coefficient. A black body absorbs all heat radiation with all wavelengths from all directions[26]. The consideration of a black body is idealized. For the illustration of a real body (see Equation 2.9), the emissivity ϵ is used. ϵ is material-dependent and lies between 0 and 1.

$$\dot{q} = \epsilon \sigma T^4 \quad (2.9)$$

2. Foundations

In general, a body absorbs, transmits, and reflects radiation with the appropriate coefficients a , τ and r . The sum of three coefficients has to be one ($a + \tau + r = 1$) [27].

The primary source of heat radiation is the sun, which plays an important role in the thermal modelling of buildings. Objectives in the building, such as radiators, also radiate heat. For example, radiators have equal parts convective and radiative energy transport [28].

2.2. Lumped capacitance model

For modelling the thermal behaviour of buildings, the lumped capacitance model is often used. With this approach, using the electrical analogy, building elements are represented by resistors R and capacitors C [11].

2.2.1. Electrical analogy

Similar to an electrical network, the potential is represented by the temperature at one node and the heat flux corresponds to the current. In analogy to the electric domain, we can describe the Ohm's law in heat transfer by:

$$\dot{Q} = \frac{\Delta T}{R} \quad (2.10)$$

Combining the above equation with Equation 2.6 or Equation 2.7, the thermal resistance R is determined in conductive cases as [25]:

$$R_\lambda = \frac{d}{A\lambda} \quad (2.11)$$

and in convective cases as [26]:

$$R_\alpha = \frac{1}{\alpha A} \quad (2.12)$$

2. Foundations

Thermal resistances can be summarised to one thermal resistance, even if they are from different mechanisms of heat transfer. Based on an example in Figure 2.1, the addition is explained. The figure shows a section of a wall with a heat flow \dot{Q} , the ambient temperature T_1 and T_2 separated by that wall. We have three thermal resistances $R_{\alpha,1}$, $R_{\alpha,2}$, and R_λ , which we sum to one thermal resistance $R = R_{\alpha,1} + R_\lambda + R_{\alpha,2}$. Now, we can calculate the heat flow $\dot{Q} = \frac{T_2 - T_1}{R}$ according to Equation 2.10.

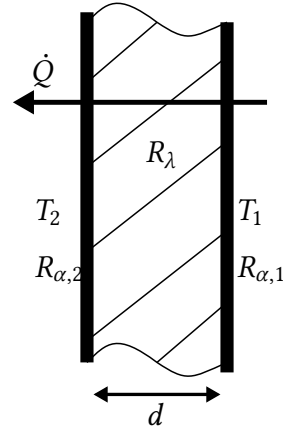


Figure 2.1. Sample of a wall with thermal resistances

In sum, the thermal resistances R comply with electrical resistors. Further for modelling thermal networks, the thermal capacitance C is needed. It is calculated from the specific heat capacity c multiplied by the mass m ($C = cm$).

For a better explanation of the structure of a thermal network, a simple example is depicted in Figure 2.2. It represents a heated wall of a building. The heat flux \dot{Q} , for example from a

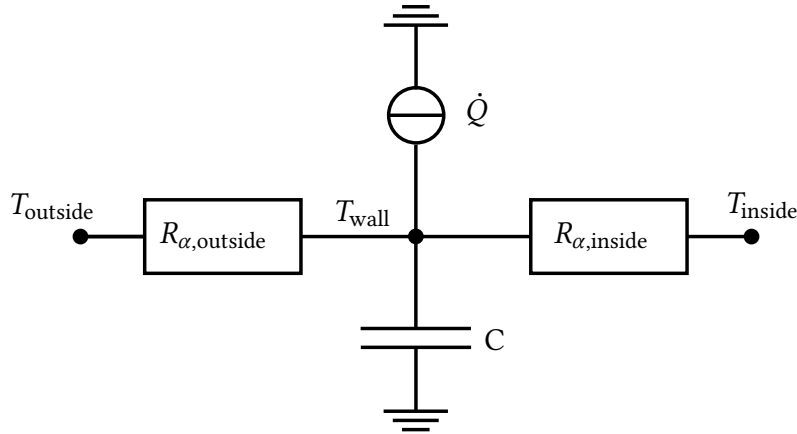


Figure 2.2. Sample RC- network

radiator, influences the temperature T_{wall} , as well as the capacitance C . And the temperature T_{wall} affects the temperature inside and outside T_{inside} and T_{outside} with their resistances $R_{\alpha,\text{inside}}$ and $R_{\alpha,\text{outside}}$. The example shows that all connections in the network influence each other. To

2. Foundations

model the dynamics of the wall in differential equations, Kirchhoff's Current Law is required. It states that the sum of the flowing current to the node is equal to the sum of the flowing current of the node [25]. Because of the thermal analogy of electrical laws, the current is replaced by heat flux. The following differential equation results for the node T_{wall} using Ohm's law ($\dot{Q} = \Delta T/R$) and the first law of thermodynamics as deduced in Equation 2.2 with the inner energy from Equation 2.4.

$$C \frac{dT_{\text{wall}}}{dt} = \dot{Q} + \frac{T_{\text{inside}} - T_{\text{wall}}}{R_{\alpha,\text{inside}}} - \frac{T_{\text{wall}} - T_{\text{outside}}}{R_{\alpha,\text{outside}}} \quad (2.13)$$

In Figure 2.2, the thermal resistances are serially connected. According to the electrical network, resistances in series are equal to their sum.

$$R_{\text{sum}} = R_{\alpha,\text{inside}} + R_{\alpha,\text{outside}} \quad (2.14)$$

A parallel circuitry has windows and walls in buildings, for example. Here the resistances are calculated according to the following schema:

$$\frac{1}{R_{\text{sum}}} = \frac{1}{R_{\text{wall}}} + \frac{1}{R_{\text{window}}} \quad (2.15)$$

In terms of needed more capacitances for describing the thermal model, the summary capacitance is added in a parallel circuitry as:

$$C_{\text{sum}} = \sum_1^i C_i \quad (2.16)$$

The serial circuitry of capacitances is calculated as follows:

$$\frac{1}{C_{\text{sum}}} = \sum_1^i \frac{1}{C_i} \quad (2.17)$$

2.3. Model predictive control (MPC)

Model predictive control exploits models of the plant to predict and optimise the behaviour of the plant [29]. Applied to thermal control of a building with the aim of grid-supporting, a model of the thermal behaviour of the building is required to predict the reaction of the

2. Foundations

system behaviour in the next N time steps, called the prediction horizon. Every time step k , the current state \mathbf{x}_k , the output y_k is measured, and the future system behaviour is obtained by computation. The computation of the future system behaviour may include measurable disturbances \mathbf{d}_k such as weather forecast, occupancy schedule and the optimisation of the control signal \mathbf{u}_k over the optimisation horizon \mathbf{u}_{k+N} . However, only the first calculated control signal is adopted as input for the plant. Then, the calculations are repeated at every time step. Figure 2.3 visualises the MPC control loop.

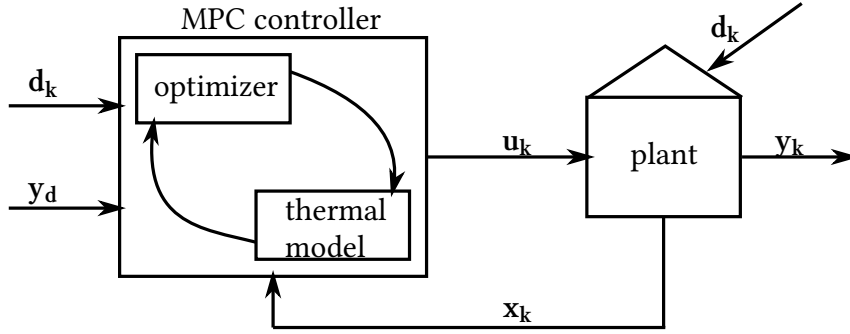


Figure 2.3. MPC structure of the control loop

Concluded, the MPC is "an iterative online optimisation over the predictions" [29] compiled by the thermal model of the building. Mathematically explained, the optimizer needs to minimize the following equation according to [30] and [31]:

$$\text{Cost function} \quad \text{minimize} \quad \sum_{k=1}^{N-1} c_k(\mathbf{x}_k, \mathbf{u}_k, y_k) \quad (2.18)$$

subject to

Current state	$\mathbf{x}_0 =$	\mathbf{x}	
Dynamics	$\mathbf{x}_{k+1} =$	$f(\mathbf{x}_k, \mathbf{u}_k, \mathbf{d}_k),$	$y_k = g(\mathbf{x}_k, \mathbf{u}_k, \mathbf{d}_k)$
Constraints	$y_{\min} \leq$	$y_k \leq y_{\max}$	
	$\mathbf{u}_{\min} \leq$	$\mathbf{u}_k \leq \mathbf{u}_{\max}$	

c_k represents the cost function, which is explained in detail in subsection 2.3.1 . In terms of building control, y is the internal temperature.

2. Foundations

	m	n
A	number of states	number of states
B_1	number of states	number of control signals
B_2	number of states	number of disturbances
C	number of outputs	number of states
D_1	number of outputs	number of control signals
D_2	number of outputs	number of disturbances

Table 2.1. dimensions of the matrices

2.3.1. Cost function

Generally, the cost function c_k assigns a cost to the control signal \mathbf{u}_k and the current state \mathbf{x}_k , which is mathematically described in Equation 2.18 , with:

$$c_k = (\mathbf{x}_k^T Q \mathbf{x}_k + \mathbf{u}_k^T R \mathbf{u}_k) \quad (2.19)$$

Here Q and R are matrices over which individual elements of the state vector or control signal vector can be weighted differently. [32] Especially for every application, the cost function has an individual form to reach the aims of the MPC.

2.3.2. Dynamics

The state-space formulation (SSF) is an alternative representation of a linear differential equation, which models a physical system. In this work, it is used for the formulation of the thermal model, which is required for the MPC. The SSF consists of the state \mathbf{x} , the control signal \mathbf{u} , the disturbances \mathbf{d} and the output of the system \mathbf{y} are represented in Equation 2.20. The system matrix is A , B_1 and B_2 are called the input matrices, C is the output matrix, D_1 and D_2 are the pass-through matrices. The Table 2.1 lists the dimensions of the matrices $m \times n$ with m rows and n columns.

$$\begin{aligned} \dot{\mathbf{x}} &= A\mathbf{x} + B_1\mathbf{u} + B_2\mathbf{d} \\ \mathbf{y} &= C\mathbf{x} + D_1\mathbf{u} + D_2\mathbf{d} \end{aligned} \quad (2.20)$$

Every differential equation needs initial values for solving. Therefore, initial states \mathbf{x}_0 , initial control signals \mathbf{u}_0 , and initial disturbances \mathbf{d}_0 must be given. In a thermal model of a building, some authors ([28], [33]) use the state as a vector of some temperatures, the control

2. Foundations

signal as a signal for the heating system, the disturbances can describe the influence by the weather or occupants and the output of the system contains frequently the temperature inside of the building.

2.3.3. Constraints

Dealing with constraints is one of the most important advantages of MPC. Thereby, constraints can be used for the state, the output, and the input. In terms of building control, output constraints and input constraints are reasonable, as mathematically described in the Equation 2.18. That means, the output constraints could be a temperature range, which feels comfortable for occupants. And the constraints for the input are given as minimal ($= 0$) and maximal values of the possible performances. General, logical and physical ranges are constrained. There are different forms of constraints, but linear constraints are frequently used for MPC because they simplify the optimisation problem. Constraints can also be time dependant. This is beneficial for embedding diverse temperature ranges during the night and the day or during the working time of occupants when they are not at home. [33]

2.4. The reference building

Since this thesis is based on a real building, the necessary details about the building will be described below. The building is located on the "Campus Nord" of the KIT and is part of the "Energy Lab 2.0", "a research infrastructure for renewable energy"[34]. It is equipped with a kitchen, a bathroom, five rooms and a technical room. For a better orientation, Figure 2.4 shows a part of the construction plan of the building. The building is designed as a single-family house, but for practical reasons, it is used as an office. The living area is around 100 m^2 . The building offers two options to heat or cool with a ground-source heat pump or an air heat pump. The focus is on the air heat pump because the most commonly used heat pumps in Germany are air heat pumps [35]. In addition to the heat pump, there is a water reservoir for saving energy with stratified storage. The total volume is 1000 litres [36]. The heating system inside the building is provided as underground floor heating. However, the heating system is not completely installed yet. So using the heat pump, the water reservoir or the underground floor heating is not possible, yet.

One of the main features of the building is the number of sensors. The air temperature is measured in every room, as well as the temperature in the middle of the exterior walls,

2. Foundations

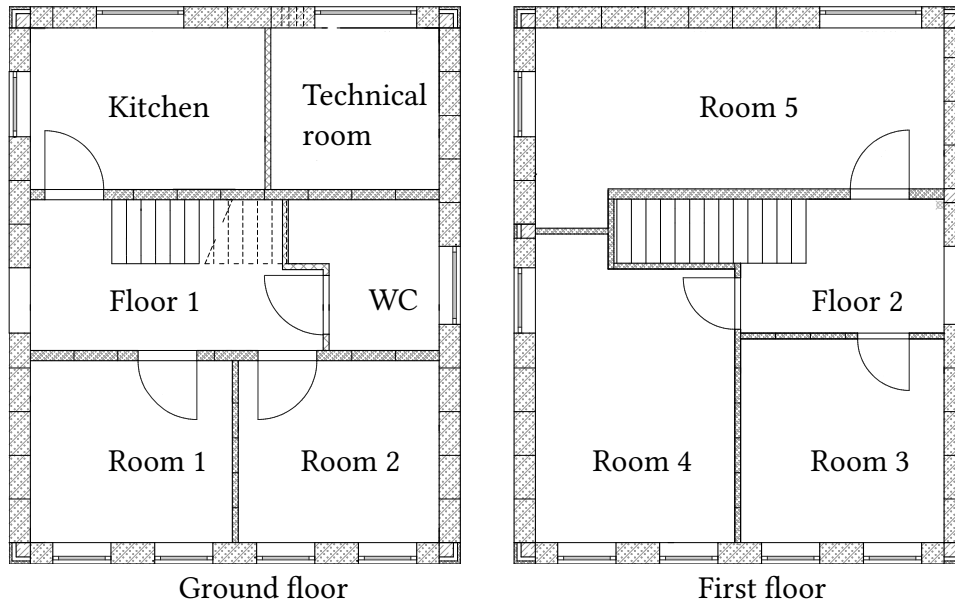


Figure 2.4. Construction plan of the building [37]

the screed temperature, the floor plate temperature, and the temperature of the inner wall between room three and room four (see Figure 2.4). Furthermore, the consumption of the actual electrical power is also detected. Only the mentioned sensors are needed in this case, but there are many more sensors.

3. Modelling

After explaining thermal basics and the electrical analogy, these foundations are used in this chapter. The development process and the results of the thermal model of the reference building will be presented. Later, the model is needed for the MPC to predict the thermal reactions of the building.

The focus of this work is on the MPC part, so a simple thermal model is required. Nevertheless, no necessary information should be missing: (i) the thermal storage possibilities, (ii) the temperature inside of the building, and (iii) the influence of the heating system. The storage allows heating during the grid has too much power and saving energy in the building, during the grid requires power. This achieves the MPC's goal of providing grid services. The output of the model needs to be the temperature inside since the MPC aims to be in a pleasant temperature range to ensure customer comfort. Finally, the influence of the heating system must be visible in the model, as it is the input of the system.

The thermal model reflects the thermal conditions of the reference building. Therefore, the inner energy of the water reservoir and the air temperature inside the building are modelled. The water reservoir and the building behaviour are modelled according to different modelling strategies. The following chapters describe the submodels water reservoir and building model, the kind of modelling, and the conclusion of the submodels.

3.1. The modelling strategies

We can create a model according to three approaches, the so-called white-box models, grey-box models or black-box models. White-box models describe the system only physically. Black-box models, on the other hand, have no physical description. They are created with data. And grey-box models are in between these two options [38]. All approaches are used in the thermal modelling of buildings [11].

3. Modelling

The chosen approach for the MPC is the **grey-box model** for two reasons: First, this approach combines the advantages of white-box models and black-box models [39]. Second, there is the possibility to generate the required data from the reference building with the available measurement equipment at KIT. According to Coakley et al., further advantages and disadvantages are among other things[15]:

Advantages	Disadvantages
<ul style="list-style-type: none"> • faster development by a combination of physical and statistical model • accuracy of the results for the specific use case, provided by qualitative training data 	<ul style="list-style-type: none"> • requires knowledge in physical and statistical modelling • changes at the building lead to a re-training

Table 3.1. Advantages and disadvantages of grey-box modelling

However, the water reservoir and the heating system are not in use, yet. So, no data is available for training a grey-box model. Thus, this submodel needs to be designed as a **white-box model**.

The benefits and challenges of white-box models are presented in Table 3.2 [39]).

Advantages	Disadvantages
<ul style="list-style-type: none"> • relies on physics • applicable for every situation with the same assumptions and requirements 	<ul style="list-style-type: none"> • needs assumptions to simplify • often complex mathematical problems

Table 3.2. Advantages and disadvantages of white-box modelling

3.2. The water reservoir model

For the modelling of the water reservoir (WR), all heat flows that influence the water reservoir are first considered (see Figure 3.1). The heat pump (HP) feeds the water reservoir with heat flow \dot{Q}_{HP} . The service water (SW) and the water for the heating circuit are removed from the storage. Since no service water is currently connected to the reference building, the heat flow \dot{Q}_{SW} will be set to zero in the following. The heat losses \dot{Q}_{loss} and the heating heat flow $\dot{Q}_{heating}$ are consequently the discharged heat flows. The resulting energy balance according to Equation 2.1 follows below.

$$\frac{dU_{WR}}{dt} = -\dot{Q}_{heating} + \dot{Q}_{HP} - \dot{Q}_{loss} \quad (3.1)$$

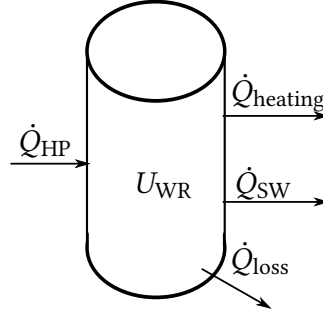


Figure 3.1. Figure of the water reservoir with the heat flows

Since the model relates to a real building, the size of the heat flows and the inner energy are limited according to the devices of the building. The heating heat flow is in a range according to the calculations of the heating system [40] and can also have negative values when cooling is required (then according to the calculations of the cooling load [41]). The heat losses and the heat pump heat range are taken from the technical data [36], [42].

Since the reference water reservoir is a stratified storage we determine the maximum inner energy in assumption of two heat layers. According to Equation 2.4, we need material parameters of water ($c_{v,w}$, ρ_w), the size of the water reservoir ($m = \rho_w V$), both is known, and a temperature difference, which we define for both layers. We assume that we heat the storage from ambient temperature T_{amb} around 20°C in both layers. Even with negative outside temperatures, the characteristic diagram of the heat pump provides the maximum inlet temperature of 55 °C, which should be the maximum temperature of the upper layer in the water reservoir $T_{max,1}$. The maximum temperature of the lower layer $T_{max,2}$ is based on

3. Modelling

the inlet temperature of the underfloor heating and lies by 35 °C. After that, we calculate the sum of the inner energy as follows.

$$U = \rho_w c_{v,w} ((T_{\max,1} - T_{\text{amb}}) \cdot \frac{V}{2} + (T_{\max,2} - T_{\text{amb}}) \cdot \frac{V}{2}) \quad (3.2)$$

3.3. The building model

First, the thermal dynamics of the building must be described physically. To comply with the requirement of a simple model, we model the building as a single zone, as often practised in the literature [43], [28]. Single zone means that we sum the values of interest of the rooms, such as air temperature or wall temperature, by averaging to one value.

We consider the air temperature, the temperature of the outer walls, the temperature of the inner walls and floors in the first floor, and the temperature of the floor in the model. In the following, these temperatures are called: inside temperature T_{inside} , envelope temperature T_{envelope} , interior temperature T_{interior} , and floor temperature T_{floor} . Using the state-space formulation (see subsection 2.3.2), the temperatures are states in this model. According to the RC-analogy (see subsection 2.2.1), the model is built and explained in more detail in the following for every state.

Inside temperature:

The accuracy of the inside temperature is focused since this temperature will be controlled in the later prepared MPC. Therefore, a more precise description of the dynamics is required (see the following equation). We consider the influence of the sun $\dot{Q}_{\text{sun,inside}}$, the heating system \dot{Q}_{heating} and the other states in the way shown in the following equation. \dot{Q}_{heating} links the water reservoir model and the building model because the heat flow is the same but leaves the water reservoir model and enters the building model.

$$C_{\text{inside}} \cdot \frac{dT_{\text{inside}}}{dt} = \dot{Q}_{\text{heating}} + \dot{Q}_{\text{sun,inside}} - \frac{T_{\text{inside}} - T_{\text{envelope}}}{R_{\text{inside}}} - \frac{T_{\text{inside}} - T_{\text{outside}}}{R_{\text{window}}} - \frac{T_{\text{inside}} - T_{\text{interior}}}{R_{\text{interior}}} - \frac{T_{\text{inside}} - T_{\text{floor}}}{R_{\text{floor}}} \quad (3.3)$$

The detailed explanation for the composition of the thermal resistance and capacitance is in subsection 2.2.1. In the following table, the special material and state dependant values are explained.

3. Modelling

C_{inside}	The thermal capacitance C_{inside} is calculated with the mass of the air from all rooms and the capacity of the air ($1006 \text{ J}/(\text{kgK})$ [44]). The mass can be determined with the volume of the rooms according to the construction plan [37] and the air density ($1.28 \text{ kg}/\text{m}^3$ [44]).
R_{inside}	The thermal resistances R_{inside} includes a convective part with the transfer coefficient $\alpha = 0.9 \text{ W}/(\text{m}^2\text{K})$ special for air perpendicular to the wall in buildings with the assumption of one Kelvin temperature difference between the wall and air [45].
R_{window}	The window resistance R_{window} is determined with the window area and the assumption of a heat transmission coefficient $u = 1 \text{ W}/(\text{m}^2\text{K})$ [46].
R_{floor}	Heat conductivity and heat convection are the regarded mechanisms to determine the floor resistance R_{floor} . The floor material is reinforced concrete with the thermal conductivity of $2.3 \text{ W}/(\text{mK})$ [47].
R_{inside}	For the convection in the inner of the building, the same assumptions are made as for R_{inside} .
R_{interior}	The interior resistance R_{interior} is also calculated with the heat transfer coefficient inside.

Table 3.3. Explanation of the special material and state dependant values of the differential equation of the inside temperature

Envelope Temperature:

The envelope temperature is influenced by the sun, the contact of the walls with the inner air temperature and with the outside temperature. The sun affects the air temperature differently than the outer walls. Therefore, we difference the influence of the sun on the inner air temperature and the envelope, and we consider here $\dot{Q}_{\text{sun, envelope}}$.

$$C_{\text{envelope}} \cdot \frac{dT_{\text{envelope}}}{dt} = \dot{Q}_{\text{sun, envelope}} - \frac{T_{\text{envelope}} - T_{\text{outside}}}{R_{\text{envelope}}} + \frac{T_{\text{inside}} - T_{\text{envelope}}}{R_{\text{inside}}} \quad (3.4)$$

3. Modelling

R_{envelope}	The outer wall resistance R_{envelope} contains a heat conductivity of aerated concrete ($0,133\text{W}/(\text{mK})$ [48]) and the heat transfer coefficient for air perpendicular to the wall outside α_{envelope} according to the rules of thumb from Schweizer-fn $\alpha_{\text{envelope}} = 3.96(v/L)^{0.5} = 1.669\text{W}/(\text{m}^2\text{K})$ [45] with the average wind velocity of Karlsruhe v [49] and the length of the building wall.
C_{envelope}	To determine the capacitance C_{envelope} , we need the volume of the outer walls from the construction plan [37], the density of aerated concrete ($485\text{kg}/\text{m}^3$) and the capacity ($1000\text{J}/(\text{kgK})$) [48].

Table 3.4. Explanation of the special material and state dependant values of the differential equation of the envelope temperature

Interior and floor temperature:

The differential equations for the interior and the floor temperature are the simplest one. Both states have just an impact on the inside temperature. Hazyuk et al. [28] models also the ground floor as one state. The explanation is that the ground floor has no convective contact with the environment. Therefore, the ground floor is not modelled with the envelope for holding the physical structure, where the wind has an impact on the outer walls. The interior is modelled to improve the accuracy of the inside temperature equations because of the special collection of the capacitance of the inner walls.

$$C_{\text{interior}} \cdot \frac{dT_{\text{interior}}}{dt} = \frac{T_{\text{inside}} - T_{\text{interior}}}{R_{\text{interior}}} \quad (3.5)$$

$$C_{\text{floor}} \cdot \frac{dT_{\text{floor}}}{dt} = \frac{T_{\text{inside}} - T_{\text{floor}}}{R_{\text{floor}}} \quad (3.6)$$

As above, we have to determine the material parameters of the capacitance C_{floor} and C_{interior} . The material of the floor is reinforced concrete and the interior' material is aerated concrete. The previously unnamed material parameters are the density ($2500\text{kg}/\text{m}^3$) [47] and the capacity ($880\text{J}/(\text{kgK})$) [50] of reinforced concrete.

Summarising, Figure 3.2 illustrates the building model with all its connections according to the RC- analogy.

3. Modelling

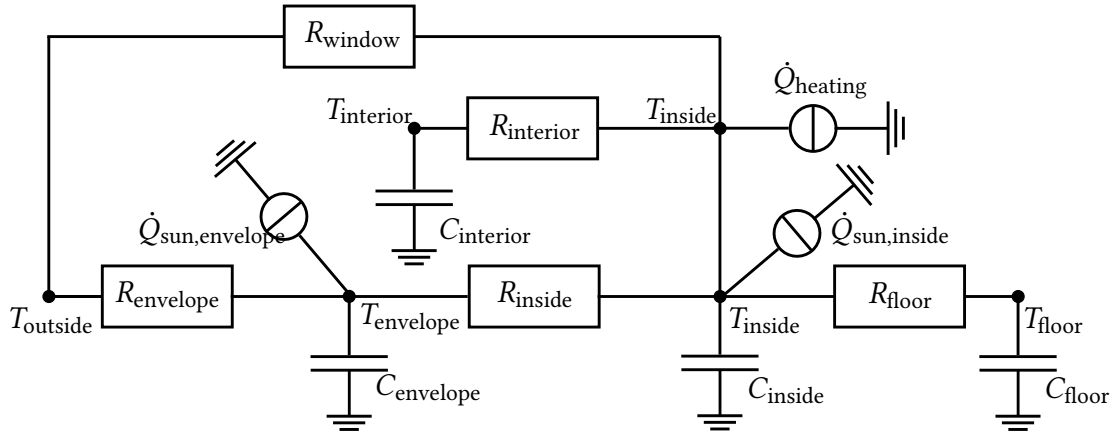


Figure 3.2. Structure of the thermal model in RC- analogy

3.3.1. Parameter identification

Figure 3.3 explains the procedure, how to generate the grey-box model from the physical building model.

The used toolbox from Matlab is the "System Identification Toolbox". For this application,

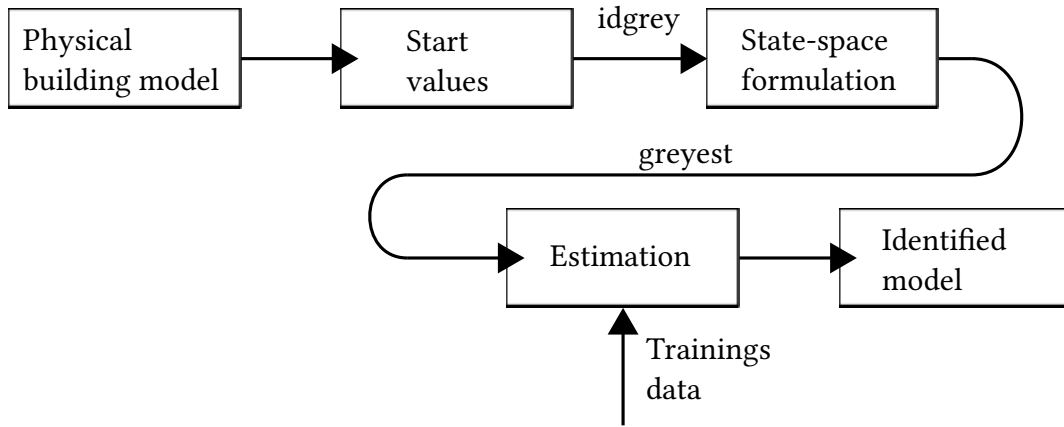


Figure 3.3. Workflow of grey-box modelling with Matlab

the most important commands are "idgrey" and "greyest". With the idgrey-command, we can specify the building model as the initial model for the grey-box estimation in state-space formulation. That means the thermal resistances and capacitance, which we determined above, are the start values for the estimation and they are the values, which the estimator from Matlab can vary. We also identify the parameters $f_{sol,inside}$ and $f_{sol,envlope}$ because we

3. Modelling

model in the simplest way the heat flow of the sun isolation $\dot{Q}_{\text{sun, envelope}}$ and $\dot{Q}_{\text{sun, inside}}$ with the measured diffuse insolation I_{sun} (see the following equation).

$$\begin{aligned}\dot{Q}_{\text{sun, inside}} &= f_{\text{sol, inside}} I_{\text{sun}} \\ \dot{Q}_{\text{sun, envelope}} &= f_{\text{sol, envelope}} I_{\text{sun}}\end{aligned}\tag{3.7}$$

The start values for $f_{\text{sol, inside}}$ and $f_{\text{sol, envelope}}$ are chosen as 0.25 according to Harb et al. [12]. And, we replace in the differential equation of the envelope temperature from Equation 3.4 the thermal resistance R_{inside} to R_{in} . The start values of R_{inside} and R_{in} are the same, but we obtain more flexibility in the grey-box model, if we estimate both values.

After that, After that, we look for the data from the reference building. The data is generated in an experiment, as explained in a subsequent chapter. When we have the data, it is separated into training data and verification data. The training data is used for the estimation. From the reference building, we obtain the room temperatures, which we average with the capacitance of each room to one value, the inside temperature. The same procedure is adopted for the outer wall temperature, except that the outer wall temperatures are averaged with their own capacitance. The interior and the floor temperatures are determined in the same way. Also, we obtain data of the heating system for \dot{Q}_{heating} and the weather (the outside temperature T_{outside} and the diffuse insolation I_{sun}).

Now, the greyest-command executes the parameter identification with the training data. The used search method of the greyest-command is subspace Gauss-Newton least squares search, an algorithm which minimises non-linear functions [51]. The table below summarises the modelling parameters for the estimation. The states T_{inside} and T_{envelope} are also defined as the output to be optimised. For the later MPC, T_{inside} is the only relevant output. However, when optimising the two states with the more complex differential equations, we expect better results for the overall model due to the better physical description. At last, we obtain the ready model (see in section A.1 the start values and the identified values).

3.3.2. Training and verification of the thermal model

The training data set comprise twelve days from 23 July to 4 August 2021, including a heating period from 26 July to 1 August 2021. The verification data set is half the size of the training data set (from 13 July to 19 July 2021), also including a heating period from 16 July to 18 July 2021.

3. Modelling

Parameters to be identified	$C_{\text{inside}}, C_{\text{envelope}}, C_{\text{interior}}, C_{\text{floor}}, R_{\text{inside}}, R_{\text{window}}, R_{\text{envelope}}, R_{\text{interior}}, R_{\text{floor}}, R_{\text{in}}, f_{\text{sol,inside}}, f_{\text{sol,envelope}}$
Inputs	$\dot{Q}_{\text{heating}}, I_{\text{sun}}, T_{\text{outside}}$
Outputs to be optimised	$T_{\text{inside}}, T_{\text{envelope}}$

Table 3.5. Conclusion of relevant information about the grey-box model

Figure 3.4 and Figure 3.5 show the curve of the inside temperature of the simulated and the

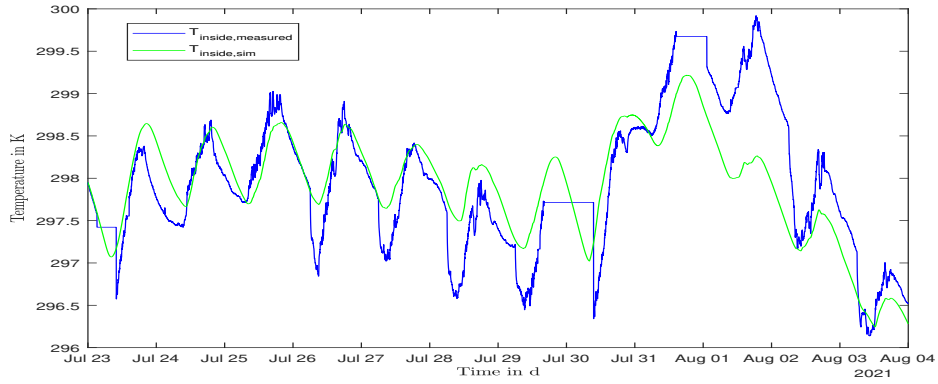


Figure 3.4. Training of the building model

measured values for the training and verification period. The use of data from a occupied building leads to the difference between the model and the measured inside temperature. The required simple model can not consider random influences such as opening doors and windows, the number of occupants, and the electric consumption in the building. Nevertheless, it is noticeable that the model reflects the dynamic of reality sufficiently. In addition, the Root Mean Square Error (RMSE) and the maximum residual (R_{max}) is used as verification measure of the model.

The RMSE is calculated with the quadratic difference of the simulated output y_{sim} and the measured output y_{meas} as follows [52]:

$$RMSE = \sqrt{\frac{1}{N} \sum_{i=1}^N (y_{\text{sim}} - y_{\text{meas}})^2} \quad (3.8)$$

3. Modelling

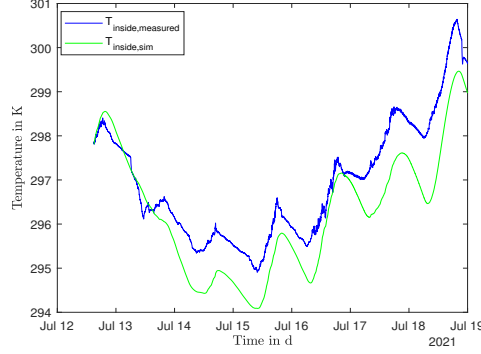


Figure 3.5. Verification of the building model

Here is N the number of measurements or simulated values. Based on the Figure 3.6 presented RSME and R_{\max} , it can be shown that during the training and verification period, the magnitudes of the RSME and R_{\max} are similar. The results of the RMSE and the R_{\max} are listed for the two optimised outputs after the training and the verification period. The maximum

	T_{inside}		T_{envelope}		
RMSE	0.52 K	0.84 K	0.49 K	0.51 K	Training period
R_{\max}	1.66 K	1.92 K	1.21 K	1.00 K	Verification period

Figure 3.6. RMSE and R_{\max} of the output for training and verification period

difference between the training and verification period for the RMSE lies by 0.32 K and for the R_{\max} by 0.26 K. As a result, we can verify the building model.

3.4. The state-space formulation

The white-box model of the water reservoir and the grey-box model of the building behaviour have now been prepared. In the next step, we put them together in the state-space formulation, which we introduced in subsection 2.3.2, just as the MPC requires.

The separation in control signal \mathbf{u} and disturbances \mathbf{d} is important for this. The control signals are the heat flow of the heating system \dot{Q}_{heating} and the heat pump in the reference building

3. Modelling

\dot{Q}_{HP} . The main disturbances are the weather and, especially for the water reservoir, heat losses. Therefore, the state-space formulation results as follows:

$$\begin{pmatrix} \frac{dT_{\text{inside}}}{dt} \\ \frac{dT_{\text{envelope}}}{dt} \\ \frac{dT_{\text{interior}}}{dt} \\ \frac{dT_{\text{floor}}}{dt} \\ \frac{dU_{\text{WR}}}{dt} \end{pmatrix} = A \begin{pmatrix} T_{\text{inside}} \\ T_{\text{envelope}} \\ T_{\text{interior}} \\ T_{\text{floor}} \\ U_{\text{WR}} \end{pmatrix} + B_1 \begin{pmatrix} \dot{Q}_{\text{heating}} \\ \dot{Q}_{\text{HP}} \end{pmatrix} + B_2 \begin{pmatrix} I_{\text{sun,inside}} \\ I_{\text{sun,envelope}} \\ T_{\text{outside}} \\ \dot{Q}_{\text{loss}} \end{pmatrix} \quad (3.9)$$

$$T_{\text{inside}} = C \begin{pmatrix} T_{\text{inside}} \\ T_{\text{envelope}} \\ T_{\text{interior}} \\ T_{\text{floor}} \\ U_{\text{WR}} \end{pmatrix}$$

The complete matrices A , B_1 , B_2 , and C are presented in section A.2. We have no pass-through matrices D_1 or D_2 because neither control signals nor disturbances have a direct impact on the output.

4. Experiments

In section 3.3 is described how the grey-box model of the building is created. However, it is not precise explained where the data comes from. Experiments have been conducted specifically to obtain this data. These experiments are explained in this separate chapter.

This thesis is developed during the summer, thus no data from the reference building with a non-zero control signal \dot{Q}_{heating} are available. To acquire data with the varying control signal, we heat the reference building with electric heaters in two experiments, one for the verification data and one for the training data. Therefore, the sensors of the building record the temperature curves in the rooms and the electrical consumption of the building. The experiments are under the assumption that the whole electrical power of the heaters and other consumers of power, such as lights and office devices, is converted in heat.

4.1. Experiment 1

The feasibility of the first experiment on the reference building is unclear. To be able to simply repeat the experiment in the event of an error, the experiment with the smaller data set is conducted at first. Hence, the first experiment aims to obtain the data for the verification period, which is shorter than the training period. Furthermore, the experiment is conducted over a weekend (from 16. July to 18. July 2021), as we reduce interference from occupants, such as opening doors or windows, and we enable the occupants a comfortable working temperature. Therefore, all windows and doors are opened after the experiment to cool down the building. At last, there should be no electrical charging of the cars during the experiment, because this electricity consumption has the same measuring point as the electricity consumption of the entire building. This would disrupt the assumption that all electrical power is converted into heat.

At first, we set up the household heater without a fan in room 1, the household heater with a fan in room 2, and the industrial heater in floor 2 (see Figure 2.4). The heaters are

4. Experiments

Heater	Acronym	Technical data	Configuration
Household Heater without a Fan	HoHe	<ul style="list-style-type: none"> • maximum power: 2000W • closed-loop control 	<ul style="list-style-type: none"> • switch symbol: • temperature setting: 5 – 6
Household Heater with a Fan	HoHeF	<ul style="list-style-type: none"> • maximum power: 2000W • open-loop control 	<ul style="list-style-type: none"> • switch symbol: 750W
Industrial Heater	IH	<ul style="list-style-type: none"> • maximum power: 9000W • closed-loop control • three phase 	<ul style="list-style-type: none"> • switch symbol: ■ • temperature setting: middle

Table 4.1. Technical data and configuration during the experiments [53], [54], [55]

selected based on availability so that no new equipment has to be purchased. Some technical information and the configuration of the heaters are described in Table 4.1.

4.1.1. Data of the experiment 1

A more exact sequence of the experiment is showing in Table A.2 as laboratory journal or in Figure 4.1 with the data. The Figure presents the electrical consumption P_{el} and the air temperatures in rooms 1 and 2, the kitchen, and floor 2 of the reference building from the beginning to the ending of the experiment. The start is marked by switching on the heaters in floor 2 and rooms 1 and 2. In the end, the heaters are switched off in room 1, the kitchen and floor 2.

The data demonstrate the behaviour of the heaters. Consequently, in floor 2, the IH switches often on and off due to the closed-loop control. Therefore, IH generates the fluctuations in the increasing air temperature curve. At the same time, we notice the on and off of the heater in P_{el} at the high peaks. The HoHe has the same behaviour as the IH but with a smaller influence on the air temperature in room 1 due to its lower power.

Only the HoHeF is controlled open-loop and heats constantly with 750W the room air, where

4. Experiments

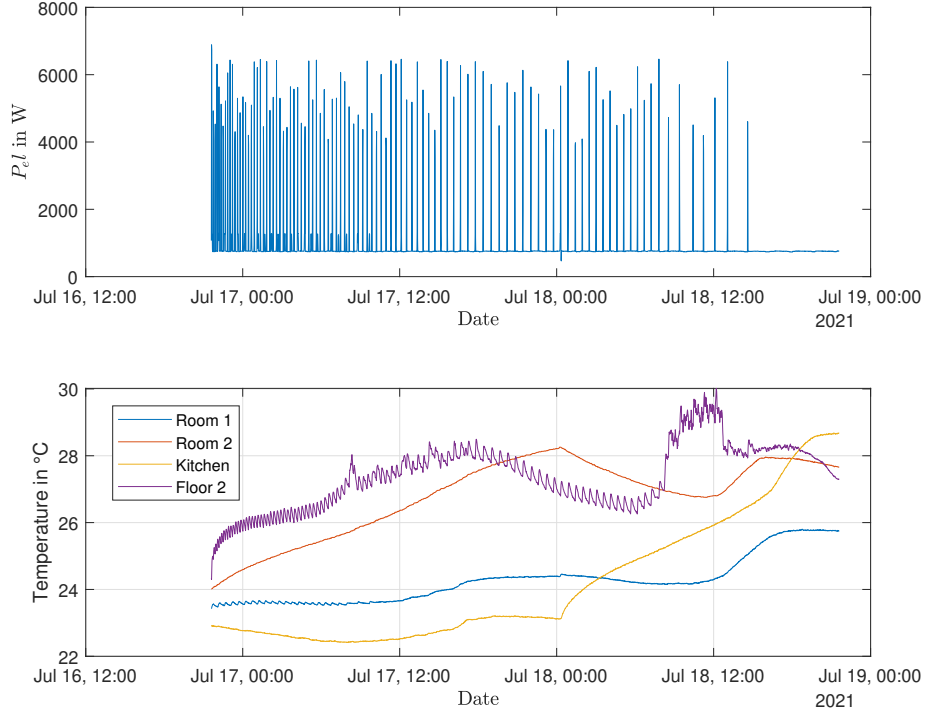


Figure 4.1. Electrical consumption of the building and air temperature inside the rooms during the experiment 1

we remark no fluctuations in the temperature rise. Because the HoHeF does not switch off independently and we have sunny days during the experiment, some temperatures, e.g. the screed temperature, are nearly below 40°C. To avoid a too-hot room for the occupants after the experiment, we stop heating room 2 on Saturday night and rearrange the HoHeF in the kitchen. Since we average the temperature in all rooms for the model estimation from chapter 3, it is not relevant which room is heated.

4.2. Experiment 2

Experiment 2 roots also on the general assumption of converting the entire electrical power to heat, and starts on Monday, 26. July 2021 and ends on Sunday night, 1. August 2021. We use also the heaters explained in Table 4.1. In contrast to experiment 1, we can now remotely control the switching on and off of the heaters due to an update in the building. Therefore, we can generate more training data by controlling heating periods on working days during the

4. Experiments

night and on the weekend. In order not to burden the occupants during the working day, we heat at night and only the unused kitchen with the HoHeF. In addition, we can use another measuring point for the electrical consumption during the working days, where the electric car charging is not considered. Only for the weekend, we need both measuring points (the one only used in experiment 1 and the new one used during the working days in experiment 2) to measure the whole energy consumption because of the three-phase connection of the IH, which is measured at the same point as car charging. So, we have to ensure no car charging during the weekend. Besides, the heaters are in the same rooms as in experiment 1 over the weekend. Table A.3 or the data describe the incidences during experiment 2, which is explained in detail in the next section.

4.2.1. Data of the experiment 2

Figure 4.2 presents the needed electrical consumption and the air temperatures of the rooms of interest during experiment 2. Especially, the air temperature of the kitchen is showed over the whole experimental phase because in the first five days only this room is heated for reasons explained above. The heating periods are remarked by horizontal lines. The visible horizontal curves of the air temperatures arise from the breakdown of the programmable logic controller (PLC). During this breakdown, no temperature data can be recorded. In every heating period with a working PLC, the increasing temperatures are conspicuous. Notice the third period: The rising temperature is visible from the point at closing the door in the kitchen (compare Table A.3). When the door is open, the heat spreads in the building and, a smaller temperature rise is visible in the kitchen. In this experiment, also, the different heaters have the same effect on the air temperatures and the HoHeF is moved from room 2 to the kitchen to avoid too high temperatures at the weekend.

4. Experiments

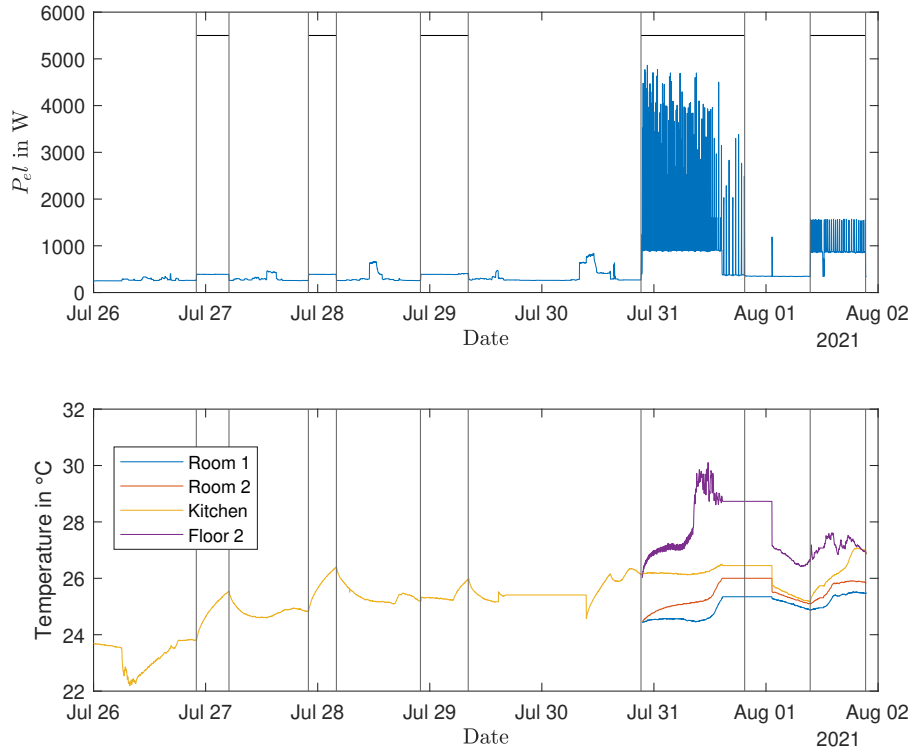


Figure 4.2. Electrical consumption of the building and air temperature inside the rooms during the experiment 2

4.3. Findings of the experiments

All influences on the building are noticeable in the data. The heating of a room directly increases the air temperature and with a time delay the wall and screed temperatures; the room temperature rises more slowly through open inner doors; the temperature curves show whether the heating is heating or not; and opening all windows and doors lead to a decreasing temperature at the end of the experiments.


No temperature data can be recorded during the PLC breakdown. This degrades the quality of the data used to estimate the model. Especially during this time, it is partially heated. Data collection would be particularly important here to determine the influence of heating. To reduce the negative impact on the data, it is important to switch off the heaters quickly in case of PLC breakdown, which is possible with remote access for the household heaters. This

4. Experiments


does not apply to the IH, as it has no remote control due to its three-phase connection and thus heats for longer periods without temperature detection.

In a look back, the use of different measuring points for electrical consumption is disadvantageous. If it seemed advantageous when considering experiment 2 that no consideration has to be given to the car charging, this actually means that the same combination of measuring points has to be used for the verification data from experiment 1, which was not planned, at first. Therefore, the model is identified with the sum of the data from both measuring points, within a period of car charging. Nevertheless, we obtain a suitable model for the MPC.




5. Model predictive control

In this chapter, the framework conditions of the MPC are described by answering the questions: (i) what is controlled? (ii) How is controlled? (iii) Which curves are controlled? (iii) What data are used? Also, the constraints, the cost function, and the workflow of the MPC script are introduced. The objective of this investigation is to obtain a control signal for the heat pump of the reference building that considers grid services and occupancy comfort. There, the investigation stays in a simulation environment 

5.1. Framework conditions of the MPC

The objective of the MPC is to optimise the control signal of the reference building $\mathbf{u} = (u_1 \ u_2)^T = (\dot{Q}_{\text{heating}} \ \dot{Q}_{\text{HP}})^T$. Thereby, we consider the heat flows of the building in the MPC simulation but, we calculate with a characteristic diagram of the heat pump the electrical control signal P_{HP} . The controlled output is the inside temperature $\mathbf{y} = T_{\text{inside}}$, which we calculate with the thermal model from section 3.4. The desired curves of the \mathbf{y} depend on the presents of occupants, which is determined on an occupancy schedule. Past data of the weather and the dynamic price of the electricity dP is used for the simulation environment.

5.1.1. Characteristic diagram of the heat pump

The characteristic diagram of the heat pump is interpolated with the characteristic values specified by the producer [42]. We assume an operation at the nominal power of the heat pump. As Figure 5.1 shows, the electrical power P_{HP} depends on the outside temperature T_{outside} and the required heat flow \dot{Q}_{HP} . Further, the heat pump can generate negative \dot{Q}_{HP} when cooling is desired. The optimisation of the MPC computed ~~the~~ \dot{Q}_{HP} , and ~~the~~ T_{outside} is known at every time step, then the characteristics of the heat pump ~~are~~  used to calculate the P_{HP} .  The optimised control signal as heat flows cannot directly influence the grid. Therefore, 

5. Model predictive control

P_{HP} is needed to analyse the effects on the grid. Furthermore, converting u into P_{HP} simplifies the analysis, as we then only consider positive values.

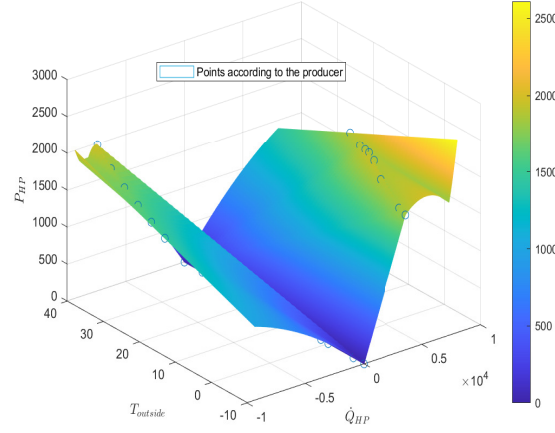


Figure 5.1. Interpolation of the characteristic diagram of the heat pump with nominal power according to [42]

5.1.2. Occupancy schedule

The Figure 5.2 presents the occupancy schedule. It summarises the working time of occupants with a green bar. We assume that persons are in the reference building from Monday to Thursday from 6 am to 7 pm and on Friday from 6 to 6 pm. The assumption is made according to experience values and means that there is a high probability that persons will be in the building during this time.

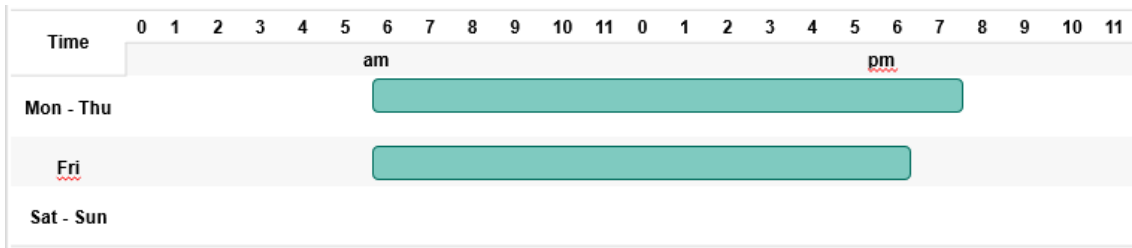


Figure 5.2. Occupancy schedule of the reference building

5. Model predictive control

5.1.3. Past data

The data used are from the same period as the training data for the model estimation. As a disturbance variable, we use the recording of diffuse radiation and outside temperature in Energy Lab 2.0. The MPC is simulated over nine days, a little more than a week, to consider the occupancy schedule at least once.

The dynamic price of the electricity dP is made available on the website of the Bundesnetzagentur [56]. Here we use the wholesale prices on the stock exchange as an indicator of grid services. The price is an intersection between supply and demand. Consequently, when the price is low, we can assume an excess of electricity on the grid. It is precisely then that it is particularly suitable to operate our heat pump to obtain electricity from the grid. In the opposite case, the same applies: If the price is high, it is unfavourable to operate the heat pump. ~~At such a time, it is particularly suitable to supply power from the grid. In the opposite case, the same applies: if the price is high, it is unfavourable to operate the heat pump.~~

However, negative prices can also arise in retail. Negative prices would undesirably change the costs of the cost function, which will be explained in more detail later at a suitable time. To avoid negative prices, we sum the absolute minimum value of the dP to every value of dP . Thus, we shift the curve of dP into positive, as shown in Figure 5.3. ~~In the later use, we calculate with~~ the dynamic price of electricity dP in the unit of $\frac{\text{€}}{\text{Wh}}$.

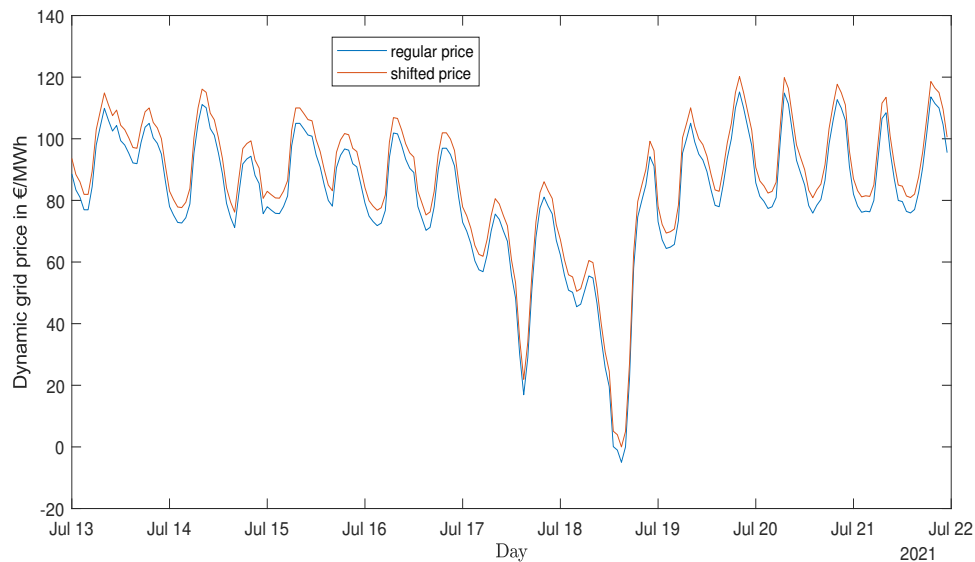


Figure 5.3. Dynamic price of electricity [56] and shifted dynamic price of electricity

5.2. The Constraints

The constraints depend on the physical limitations of the installations in the building, such as the heat pump, the underground floor heating, and the water reservoir, or of comfortable reasons. Also, the integration method of the model is included in the constraints. The subsequent section gives an overview of the constraints.

5.2.1. Constraints of the control signals

The producer's specifications restrict \dot{Q}_{HP} the maximum and minimum heat flow of the heat pump for nominal power by heating with the inlet temperature of 55°C and by cooling with the inlet temperature of 18°C [42]. The maximum $\dot{Q}_{heating}$ is limited according to the underground floor heating calculation, where the set power of every room is counted and we sum it for the complete building [40]. The computation of the required cooling power predicts 2246 W needed power by 34.5°C outside temperature in July [41]. To be more flexible with higher outside temperatures, we round the minimum $\dot{Q}_{heating}$ to 2300 W.

Further, we define a constraint $u_1 \cdot u_2 \geq 0$ to avoid simultaneous heating of building and cooling of the water reservoir or reversed. That would be energy waste. The set \mathbb{U}_k summarise mathematically the constraints.

$$\mathbb{U}_k = \{\mathbf{u}_k | -2300W < \dot{Q}_{heating} < 5283W \wedge -9340W < \dot{Q}_{HP} < 8010W | u_1 \cdot u_2 \geq 0\} \quad (5.1)$$

5.2.2. Constraint of output

The Umweltbundesamt [57] recommends an inside temperature of 18°C for some rooms, such as the kitchen. We expand the recommendation to a minimum T_{inside} of 18°C for all rooms. The maximum inside temperature refers to the German technical rules for workplaces [58], wherein a maximum of 26°C as room temperature is prescribed. The slack variable η_k allows a variance of the given temperature range during a penalty in the cost function. Thus, we have a soft constraint, and we can obtain the feasibility of the optimisation problem during a deviation of the temperature range [59]. The constraint is represented in the set \mathbb{Y}_k as follows:

$$\mathbb{Y}_k = \{\mathbf{y}_k | 18^\circ\text{C} - \eta_k < T_{inside} < 26^\circ\text{C} + \eta_k\} \quad (5.2)$$

5. Model predictive control

5.2.3. Constraints of the states

The calculation of the water reservoirs maximal inner energy U_{WR} is explained in section 3.2 with Equation 3.2. The minimum U_{WR} lies by 0 J. The set $\mathbb{X}_{5,k}$ describes the constraint for the fifth element of the state vector.

$$\mathbb{X}_{5,k} = \{x_{5,k} | 0J < U_{WR} < 96370000J\} \quad (5.3)$$

A further constraint, which relates to the states, is the integration method as discussed below.

5.2.4. Integration method and its constraint

As an integration method, we use an explicit single-step method, which means that we need the values of the actual time step k to compute the next. Possible methods are the Heun's method, the Euler and the Runge-Kutta method. The decision is made in favor of the Runge-Kutta method because the fourth order makes it more precise than the methods mentioned. The following equation shows the calculation for the next time step using the Runge-Kutta method with the sample time T_s and the function $f(\mathbf{x}_k, t_k, \mathbf{u}_k, \mathbf{d}_k) = \dot{\mathbf{x}}_k$ according to the state-space formulation (see Equation 2.20) [60].

$$\begin{aligned} a_k^{(1)} &= T_s \cdot f(\mathbf{x}_k, t_k, \mathbf{u}_k, \mathbf{d}_k) \\ a_k^{(2)} &= T_s \cdot f\left(\mathbf{x}_k + \frac{a_k^{(1)}}{2}, t_k + \frac{T_s}{2}, \mathbf{u}_k, \mathbf{d}_k\right) \\ a_k^{(3)} &= T_s \cdot f\left(\mathbf{x}_k + \frac{a_k^{(2)}}{2}, t_k + \frac{T_s}{2}, \mathbf{u}_k, \mathbf{d}_k\right) \\ a_k^{(4)} &= T_s \cdot f(\mathbf{x}_k + a_k^{(3)}, t_k + T_s, \mathbf{u}_k, \mathbf{d}_k) \\ \mathbf{x}_{k+1} &= \mathbf{x}_k + \frac{1}{6} \cdot (a_k^{(1)} + 2a_k^{(2)} + 2a_k^{(3)} + a_k^{(4)}) \end{aligned} \quad (5.4)$$

The constraints accommodate the integration method for calculating the next time step according to the determined thermal model. Important to note is that the time step of the integration is chosen in accordance with the discretization of the model. The model is estimated with the discrete values of the reference building, where the measuring points are sampled every two minutes. For example, to achieve a T_s of one hour, the T_s is described

5. Model predictive control

as $30 \cdot 2\text{min}$. ~~The two minutes are already included in the model by estimation.~~ The two minutes are already included in the model due to the estimation. Therefore, we multiply the x_k by 30 to bring forward a time step of one hour. It is considered that the thermal model is composed of two submodels. The water reservoir sub-model, which is modelled using the white-box approach, requires a different conversion to advance one hour. Here we convert watts to joules per hour. In the MPC, this difference is compensated by a factor directly in the state-space formulation of the model.

5.3. The Cost function

The cost function penalise the deviation from the desired requirements. On the one hand, we have to guaranty thermal occupant comfort in the building. On the other hand, we prefer to heat with the heat pump during convenient grid service. Both subjects are represented in the cost function below.

$$\text{minimize } \sum_{k=1}^{N-1} w_1 \cdot (y_k - y_{\text{track}})^2 + w_2 \cdot (u_{2,k} \cdot dP_k)^2 + w_3 \cdot \eta_k^2 \quad (5.5)$$

A pleasant air temperature is 22°C for living rooms, working rooms, and the bathroom [57]. As discussed in chapter 3, we model the reference building as a single-zone building, wherein most rooms are working rooms. We decide to use the median temperature of all rooms of the recommended temperatures for the complete building. Thus, the desired temperature is $y_{\text{track}} = 22^\circ\text{C}$.

The expression $(y_k - y_{\text{track}})^2$ represents the comfort requirement in the cost function. The squaring of $(y_k - y_{\text{track}})$ avoid a minimising of the cost function due to negative y_k values. The same proceeding is with the expression of the grid service $(u_{2,k} \cdot dP_k)^2$. We exclude negative values of dP_k (how is explained in subsection 5.1.3) because ~~we would generate the wrong effect with a negative dP_k .~~ After squaring, the expression would maximise the cost function during a appropriate time for grid services. Without a squaring, we would support energy consumption while its not needed or we would penalise a cooling by we having a negative $u_{2,k}$.

We can adjust the preference of the requirements by the weightings w_1 and w_1 . How much deviation is allowed from the temperature range in the soft constraint is determined by the weighting w_3 .

5. Model predictive control

The size of the cost for the requirements are different. When considering the constraints, $y_k - y_{\text{track}}$ can reach a maximum deviation of 4 K (without soft constraint), while $u_{2,k} \cdot dP_k$ is in a lower order of size due to the unit $\frac{\text{€}}{\text{Wh}}$. To compensate this, a factor is introduced that gives the comfort requirement a weaker weighting in the cost function. The factor is integrated into the weighing w_1 as shown in the following table. In general, we vary the weights w_1 and w_2 of the cost function from $i = 0$ to 1 in 0.1 steps. As shown in table Table 5.1, the comfort with w_1 and the grid service with w_2 are always weighted in opposite directions.

Occupant comfort is only necessary if persons are present in the building. Therefore, we

w_1	w_2	w_3
$\frac{1}{4} \cdot i$	$i = 1 - j$	0.001

Table 5.1. Weighting factor

consider the cost function during absence without the comfort **therm** by setting w_1 to zero according to the occupancy schedule, which results in the following simplification of the cost function during absence.

$$\text{minimize } \sum_{k=1}^{N-1} w_2 \cdot (u_{2,k} \cdot dP_k)^2 + w_3 \cdot \eta_k^2 \quad (5.6)$$

The procedure aims to generate more flexibility for the objective of grid services. **This scenario with the changing cost function is the basic scenario for this thesis.**

5.4. Workflow of the MPC script

The approach in the MPC script is determined by the use of the tool CasAdi. CasADi is an open-source tool for nonlinear optimisation and algorithmic differentiation and is characterised by a symbolic framework. Especially, mixed-integer optimal control problems, such as an MPC, are of particular interest [61]. We can combine CasAdi with MATLAB through a simple import.

The figure below gives an overview of the workflow of the MPC script. First, we create the parameter, all known sizes, and the optimisation variables symbolically. Then the inequalities of the constraints are set in a loop over the prediction horizon with the symbolic variables. The cost function is also indicated symbolically for the horizon. Afterwards, the initial values for the optimiser are determined. To specify the initial state for the first MPC step, we choose

5. Model predictive control

a constant control signal $\mathbf{u}_k = [0 \ 0]^T$, a state \mathbf{x} within the temperature range, and determine with the Runge-Kutta method the curve over the horizon. A half charged water reservoir is a further assumption for the initial state. We pass the values of the initial state of the optimisation variations and the parameters to the solver. Then, the optimisation problem is solved with the Ipopt (**I**nterior **P**oint **O**ptimiser) solver, which is appropriate for large and sparse nonlinear programming [61]. As a result, we obtain the optimised \mathbf{u}_k over the horizon. Now, after each time step, a new initial state is calculated with the curves of the states and the output from the new disturbance variables and the optimum \mathbf{u}_k over the horizon.

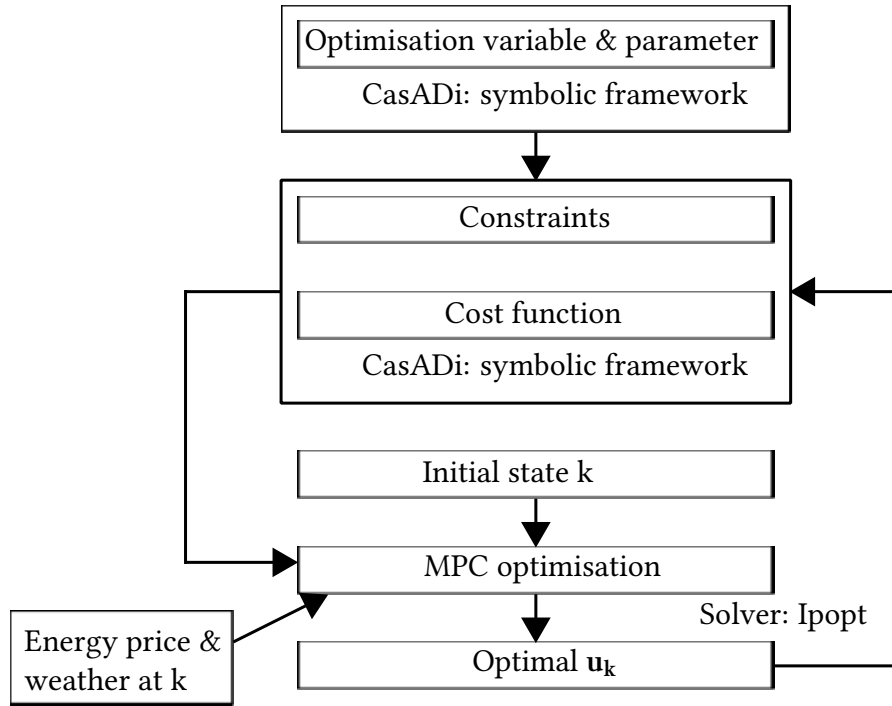


Figure 5.4. Workflow of the MPC script

5.5. Choice of weightings and horizon

In the following, we analyse the horizon length N and the effects of the weightings on the requirement of occupancy comfort and grid services for the basic scenario. For a better comparison we define an average comfort AC, which is a size of the average deviation of the y from the y_{track} over the simulation time only during presence of occupants, expressed by

5. Model predictive control

 $y_{k,occ} - y_{track}$. The calculation of AC is described in the following equation with the number of time steps with occupants n_{occ} .

$$AC = \frac{\sum_{k,occ}^{n_{occ}} |y_{k,occ} - y_{track}|}{n_{occ}} \quad (5.7)$$

On the other hand, we define the costs for grid services GS over the whole simulation time (with the number of time steps n) as the sum of the electrical power of the heat pump $P_{HP,k}$ multiplied with the dynamic price of electricity dP_k :

$$GS = \sum_k^n P_{HP,k} \cdot dP_k \quad (5.8)$$

In theoretical considerations, we should obtain a higher level of AC with less weighting of comfort and a higher level of GS with less weighting of grid services. Furthermore, a larger or shorter horizon N differs in computation time and finding the optimal solution. While a longer N requires more computation time and may not find a solution, a shorter N may not find the optimal solution. Due to finding the optimal solution a larger horizon should result in less costs for the requirements. In general, the horizon should depict the dynamics of the controlled system.

The theoretical considerations are inspected in the subsequent sections for the basic scenario over the simulation time of nine days.

5.5.1. Average comfort and grid services over the weightings

~~The following figure presents the behaviour of the AC and GS for the different weightings w_1 and w_2 with $N = 24h$. We compare the behaviour also for different horizon N to verify the feasibility and the expected behaviour. The corresponding figures are showed in section A.4 and the values of AC and GS for different horizons exposed in the following tables.~~

We notice a monotone behaviour of the average comfort and the grid services according to their weightings until small discrepancies. A possibility for discrepancies could be that the optimiser find not the global optimum. We obtain feasible solutions until for $N = 12h$ and both weightings are 0.5. The less costs with increasing horizon length is only for the average comfort notable, expecting the case $w_1 = 0$. In this case, we consider not the comfort in the cost function. Therefore, the values of AC are coincidental, also relating to the horizon length. The explanation for higher cost in GS with longer horizon is that the thermal reaction of the

5. Model predictive control

building is known over a longer time and the control signal reacts early for a better adaption of the comfort.

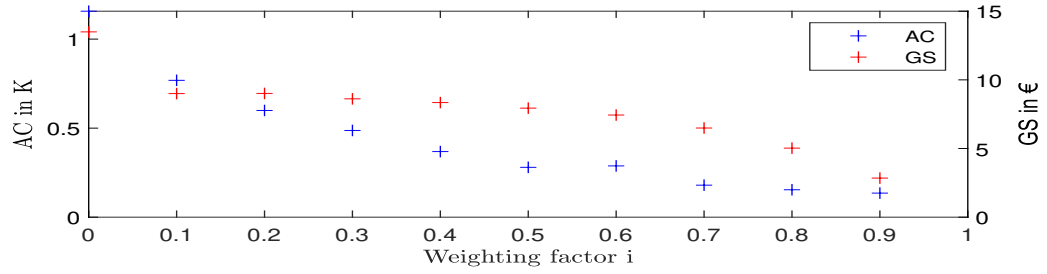


Figure 5.5. AC and GS for N = 24h

weighting factor i	0	0.1	0.2	0.3	0.4	0.5	0.6	0.7	0.8	0.9	1
AC by N = 12 h	1.11	0.89	0.77	0.64	0.54		0.40	0.28	0.24	0.22	0.22
AC by N = 18 h	1.14	0.80	0.72	0.54	0.43	0.35	0.41	0.24	0.17	0.16	0.14
AC by N = 24 h	1.16	0.77	0.60	0.49	0.37	0.28	0.29	0.18	0.15	0.14	0.20
AC by N = 30 h	1.16	0.75	0.55	0.42	0.31	0.25	0.22	0.18	0.16	0.14	0.16

Table 5.2. AC for different N

weighting factor i	0	0.1	0.2	0.3	0.4	0.5	0.6	0.7	0.8	0.9	1
GS by N = 12 h	11.97	8.31	7.90	7.35	6.93		5.23	4.37	3.12	1.71	0.00
GS by N = 18 h	16.45	9.16	8.76	8.57	7.61	7.57	6.77	5.68	4.05	2.39	0.00
GS by N = 24 h	13.50	9.00	9.01	8.62	8.35	7.94	7.44	6.49	5.03	2.85	0.00
GS by N = 30 h	13.74	8.82	8.81	8.56	8.65	8.13	7.48	6.62	5.28	3.39	0.00

Table 5.3. GS for different N

5.5.2. Choice of the horizon

The literature recommends that the predictive horizon should depict the dynamics of the system []. In this case, the temperature curves inside the reference building. Therefore, the following figure shows the T_{inside} of the building over three days determined from the measurements as a single-zone building as explained in chapter 3. We notice around every 24 h a periodic wave in the temperature curve, which is highlighted with vertical lines.

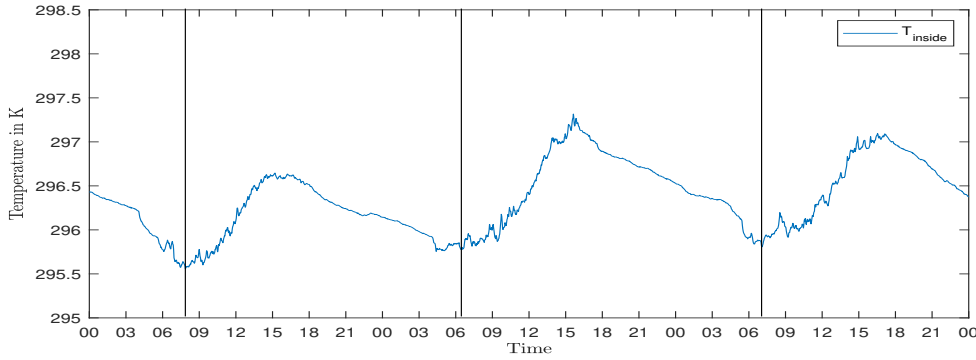


Figure 5.6. Measured data of the reference building: T_{inside} over three days

According to Figure 5.6, it is suggested to choose the predictive horizon over one day. We examine this consideration by comparing costs over different horizons for an exemplary weighting. The following figure shows the curve of costs over the simulation period. The costs here are the sum of comfort and grid services. Here, the comfort according to the occupancy schedule is only considered when the occupants are in the building. Therefore, the peaks are recognizable, and from day four to the beginning of six, there are almost no costs, as this is the weekend. The distinctions in costs at different horizons are as expected. The horizon $N = 12h$ has the highest costs, while with the longer predictions, the costs decrease. We choose the horizon of 24 h because it represents the dynamic of the reference building and the costs are partly very similar to the next longer horizon of 30 h, e.g. in the last simulation days.

5. Model predictive control

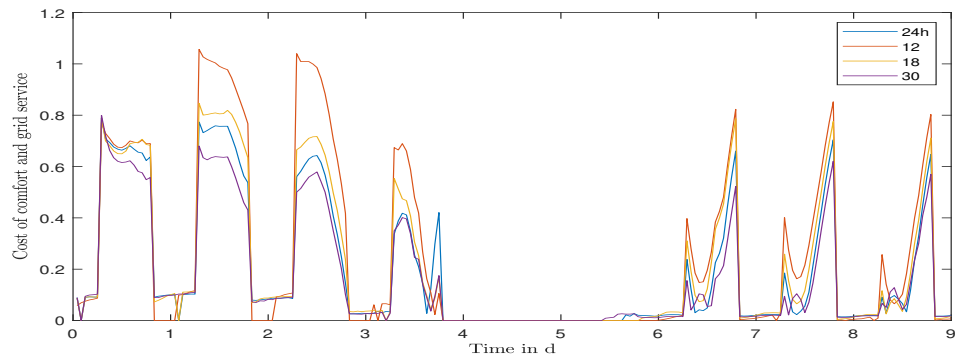


Figure 5.7. Curve of the sum of cost over simulation time for different N

6. Results

7. Conclusion

8. Outlook

Bibliography

- [1] United Nations. *Paris Agreement*. 2015.
- [2] Deutschlandfunk, ed. *Auf dem Weg zur Klimaneutralität: Die neuen Klimaziele für Deutschland*. 24.06.2021.
- [3] Bundesregierung. *Abschied von der Kohleverstromung: Fragen und Antworten*. Ed. by Presse- und Informationsamt der Bundesregierung. 2021.
- [4] C. W. Gellings. *The concept of demand-side management for electric utilities*. In: *Proceedings of the IEEE*, Vol. 73, No. 10 (1985), pp. 1468–1470.
- [5] P. Kohlhepp and V. Hagenmeyer. *Technical Potential of Buildings in Germany as Flexible Power-to-Heat Storage for Smart-Grid Operation*. In: *Energy Technology*, Vol. 5, No. 7 (2017), pp. 1084–1104.
- [6] Karl-Heinz Backhaus (Vaillant), Dr. Hendrik Ehrhardt (Stiebel Eltron), André Jacob (BWP), Barbara. *Branchenstudie 2021: Marktanalyse - Szenarien - Handlungsempfehlungen: Vorabveröffentlichung zum*. In: (24.11.2020).
- [7] F. Oldewurtel, A. Ulbig, A. Parisio, G. Andersson, and M. Morari. *Reducing peak electricity demand in building climate control using real-time pricing and model predictive control*. In: (2010), pp. 1927–1932.
- [8] I. Hazyuk, C. Ghiaus, and D. Penhouet. *Optimal temperature control of intermittently heated buildings using Model Predictive Control: Part II – Control algorithm*. In: *Building and Environment*, Vol. 51 (2012), pp. 388–394.
- [9] P. Zwickel, A. Engelmann, L. Groll, V. Hagenmeyer, D. Sauer, and T. Faulwasser. *A Comparison of Economic MPC Formulations for Thermal Building Control*. In: *2019 IEEE PES Innovative Smart Grid Technologies Europe (ISGT-Europe)*. IEEE, 29.09.2019 - 02.10.2019, pp. 1–5.
- [10] W. Wang, J. Zhang, B. Michael, and B. Futrell. *Energy Savings of Occupancy-Based Controls in Office Buildings*. In: (2019), pp. 932–939.

Bibliography

- [11] R. Kramer, J. van Schijndel, and H. Schellen. *Simplified thermal and hygric building models: A literature review*. In: *Frontiers of Architectural Research*, Vol. 1, No. 4 (2012), pp. 318–325.
- [12] H. Harb, N. Boyanov, L. Hernandez, R. Streblow, and D. Müller. *Development and validation of grey-box models for forecasting the thermal response of occupied buildings*. In: *Energy and Buildings*, Vol. 117, No. 6 (2016), pp. 199–207.
- [13] S. Freund and G. Schmitz. *Entwicklung und Validierung von Grey-Box-Modellen zur Modellierung des thermischen Verhaltens von Einzelbüros in einem Niedrigenergie-Bürogebäude*. In: (2020).
- [14] Evelyn Sperber. *Grey-Box-Modellierung des thermischen Verhaltens von Typgebäuden*. 11. Internationale Energiewirtschaftstagung. 2019.
- [15] D. Coakley, P. Raftery, and M. Keane. *A review of methods to match building energy simulation models to measured data*. In: *Renewable and Sustainable Energy Reviews*, Vol. 37 (2014), pp. 123–141.
- [16] Jiří Cigler, Jaň Sirok, Milan Korda, and Colin N Jones. *On the Selection of the Most Appropriate MPC Problem Formulation for Buildings*. In: (2013).
- [17] Danny Günther, Jeannette Wapler, Robert Langner, Sebastian Helmling, Dr.-Ing. Marek Miara, Dr.-Ing. David Fischer, Dirk Zimmermann, Tobias Wolf, Dr.-Ing. Bernhard Wille-Hausmann. *Wärmepumpen in Bestandsgebäuden: Ergebnisse aus dem Forschungsprojekt "WPsmart im Bestand": Abschlussbericht*. Ed. by Fraunhofer Institut für Solare Energiesysteme ISE. Freiburg, 2020.
- [18] M. Avci, M. Erkoç, A. Rahmani, and S. Asfour. *Model predictive HVAC load control in buildings using real-time electricity pricing*. In: *Energy and Buildings*, Vol. 60 (2013), pp. 199–209.
- [19] G. Bianchini, M. Casini, D. Pepe, A. Vicino, and G. G. Zanvettor. *An integrated model predictive control approach for optimal HVAC and energy storage operation in large-scale buildings*. In: *Applied Energy*, Vol. 240, No. 1 (2019), pp. 327–340.
- [20] D. Kim and J. E. Braun. *Hierarchical Model Predictive Control Approach for Optimal Demand Response for Small/Medium-sized Commercial Buildings*. In: (2018), pp. 5393–5398.

Bibliography

- [21] G. Bianchini, M. Casini, A. Vicino, and D. Zarrilli. *Demand-response in building heating systems: A Model Predictive Control approach*. In: *Applied Energy*, Vol. 168, No. 3 (2016), pp. 159–170.
- [22] X. Liang, T. Hong, and G. Q. Shen. *Occupancy data analytics and prediction: A case study*. In: *Building and Environment*, Vol. 102 (2016), pp. 179–192.
- [23] H. D. Baehr and S. Kabelac, eds. *Thermodynamik*. Berlin, Heidelberg: Springer Berlin Heidelberg, 2016.
- [24] *VDI-Wärmeatlas*. Berlin, Heidelberg: Springer Berlin Heidelberg, 2013.
- [25] H. Kuchling, ed. *Taschenbuch der Physik: Mit zahlreichen Tabellen*. 19., aktualisierte Aufl. München: Fachbuchverl. Leipzig im Carl-Hanser-Verl., 2007.
- [26] A. Griesinger, ed. *Wärmemanagement in der Elektronik*. Berlin, Heidelberg: Springer Berlin Heidelberg, 2019.
- [27] H. D. Baehr and K. Stephan, eds. *Wärme- und Stoffübertragung*. Berlin, Heidelberg: Springer Berlin Heidelberg, 2016.
- [28] I. Hazyuk, C. Ghiaus, and D. Penhouet. *Optimal temperature control of intermittently heated buildings using Model Predictive Control: Part I – Building modeling*. In: *Building and Environment*, Vol. 51 (2012), pp. 379–387.
- [29] L. Grüne and J. Pannek. *Nonlinear model predictive control: Theory and algorithms*. Second edition. Communications and control engineering. Cham: Springer, 2017.
- [30] J. T. Wen and S. Mishra, eds. *Intelligent Building Control Systems: A Survey of Modern Building Control and Sensing Strategies*. Advances in Industrial Control. Cham: Springer, 2018.
- [31] F. Oldewurtel, A. Parisio, C. N. Jones, D. Gyalistras, M. Gwerder, V. Stauch, B. Lehmann, and M. Morari. *Use of model predictive control and weather forecasts for energy efficient building climate control*. In: *Energy and Buildings*, Vol. 45, No. 9 (2012), pp. 15–27.
- [32] B. Kouvaritakis and M. Cannon, eds. *Model Predictive Control*. Cham: Springer International Publishing, 2016.
- [33] J. Šíroký, F. Oldewurtel, J. Cigler, and S. Prívara. *Experimental analysis of model predictive control for an energy efficient building heating system*. In: *Applied Energy*, Vol. 88, No. 9 (2011), pp. 3079–3087.

Bibliography

- [34] Karlsruher Institut für Technologie. *Energy Lab 2.0*. <https://www.elab2.kit.edu/index.php>, 15.07.2021.
- [35] Bundesverband Wärmepumpe e.V. *Positives Signal für den Klimaschutz: 40 Prozent Wachstum bei Wärmepumpen*. 19.01.2021.
- [36] ratiotherm Smart Energy Systems, ed. *Technische Daten: Oskar°Wärmepumenspeicher WPS*.
- [37] Udo Machauer. *Bauplan_ Wärmepumpenhaus*. Ed. by Karlsruher Institut für Technologie. 2017.
- [38] Statusseminar. Forschung für Energieoptimiertes Bauen, ed. *Modellbasierte Betriebsanalyse von Gebäuden - Methoden für die Fehlererkennung und Optimierung im Gebäudebetrieb*. 2009.
- [39] S. Estrada-Flores, I. Merts, B. DE Ketelaere, and J. Lammertyn. *Development and validation of "grey-box" models for refrigeration applications: A review of key concepts*. In: *International Journal of Refrigeration*, Vol. 29, No. 6 (2006), pp. 931–946.
- [40] Andreas Kejzlar. *Roth Flächentemperierung: Roth_Auslegung_Fbh*. Ed. by Roth Energiesysteme Sanitärsysteme. 21.01.2020.
- [41] SEF Ingenieurgesellschaft MBH. *KÜHLLASTBERECHNUNG VDI 2078*. 5.09.2019.
- [42] IDM ENERGIESYSTEME GMBH. *Technische Unterlagen Montageanleitung: AERO SLM 3- 11 AERO SLM 6- 17: Zusätzliche Ausstattungsvarianten HGL ohne HGL*.
- [43] H. Park, M. Ruellan, A. Bouvet, E. Monmasson, and R. Bennacer. *Thermal parameter identification of simplified building model with electric appliance*. In: *11th International Conference on Electrical Power Quality and Utilisation (EPQU)*, 2011. Piscataway, NJ: IEEE, 2011, pp. 1–6.
- [44] B. Weigand, J. Köhler, and J. VON Wolfersdorf, eds. *Thermodynamik kompakt – Formeln und Aufgaben*. Berlin, Heidelberg: Springer Berlin Heidelberg, 2016.
- [45] Anton Schweizer. *Formelsammlung und Berechnungsprogramme Maschinen- und Anlagenbau: Wärmeübergangskoeffizienten - Gase - Luft -*. Ed. by Schweizer-fn.
- [46] Thorben Frahm. *Ein Fenster mit niedrigem U-Wert spart Energie*. Ed. by D. UND Sanieren. 2021.
- [47] Anton Schweizer. *Formelsammlung und Berechnungsprogramme Maschinen- und Anlagenbau: Wärmeleitfähigkeit verschiedener Materialeien*. Ed. by Schweizer-fn. 12.10.2021.

Bibliography

- [48] K. Ghazi Wakili, E. Hugi, L. Karvonen, P. Schnewlin, and F. Winnefeld. *Thermal behaviour of autoclaved aerated concrete exposed to fire*. In: *Cement and Concrete Composites*, Vol. 62, No. 283 (2015), pp. 52–58.
- [49] Abteilung Klima- und Umweltberatung. *Jahresmittel der Windgeschwindigkeit - 10 m über Grund - in Baden-Württemberg: Statistisches Windfeldmodell (SWM)*. Offenbach, 2004.
- [50] Anton Schweizer. *Formelsammlung und Berechnungsprogramme Maschinen- und Anlagenbau: Wärmekapazität verschiedener Materialien*. Ed. by Schweizer-fn. 12.10.2021.
- [51] F. Jarre and J. Stoer, eds. *Optimierung*. Berlin, Heidelberg: Springer Berlin Heidelberg, 2019.
- [52] A. G. Barnston. *Correspondence among the Correlation, RMSE, and Heidke Forecast Verification Measures; Refinement of the Heidke Score*. In: *Weather and Forecasting*, Vol. 7, No. 4 (1992), pp. 699–709.
- [53] Thermoval Polska. *Konwektor elektryczny TX 2000, 2,0 kW, IP20, biały: Kod produktu: 5 901 812 594 495*.
- [54] Fakir-Hausgeräte GmbH. *prestige | HK 2010CT: Bedienungsanleitung Konvektor*. 2016.
- [55] Trotec GmbH. *TDS 10 / TDS 20 / TDS 30 / TDS 50: Originalbetriebsanleitung Elektroheizer*.
- [56] Bundesnetzagentur | SMARD.de. Ed. by Bundesnetzagentur für Elektrizität, Gas, Telekommunikation, Post und Eisenbahnen. www.smard.de.
- [57] Umweltbundesamt. *Richtig heizen: Richtige Raumtemperatur finden*. Ed. by Bundesrepublik Deutschland. 7.10.2021.
- [58] Bund. *Technische Regeln für Arbeitsstätten Raumtemperatur (ASR A3.5): 4.2 Lufttemperaturen in Räumen*. 2021.
- [59] J. Drgoňa, J. Arroyo, I. Cupeiro Figueroa, D. Blum, K. Arendt, D. Kim, E. P. Ollé, J. Oravec, M. Wetter, D. L. Vrabie, and L. Helsen. *All you need to know about model predictive control for buildings*. In: *Annual Reviews in Control*, Vol. 50, No. 16 (2020), pp. 190–232.
- [60] Kai Furmans, Marcus Geimer, Balazs Pritz, Carsten Proppe, ed. *Skriptum zur Vorlesung: Modellbildung und Simulation*. WS19/20.
- [61] Joel A. E. Andersson, Joris Gillis, Greg Horn, James B. Rawlings, and Moritz Diehl. *CasADi – A software framework for nonlinear optimization and optimal control*. In: (2018).

Nomenclature

Acronyms

AC	Average Comfort
DSM	Demand Side Management
GS	Costs for grid services
HoHe	Household Heater without a fan
HoHeF	Household Heater with a Fan
HP	Heat Pump
HVAC	Heating, Ventilation, and Air Conditioning
IH	Industrial Heater
KIT	Karlsruhe Institute of Technology
MPC	Model Predictive Control
PLC	Programmable Logic Controller
RMSE	Root Mean Square Error
SW	Service Water
UN	United Nations
WR	Water Reservoir

Greek letters

α	heat transfer coefficient	$W/(m^2K)$
----------	---------------------------	------------

Nomenclature

λ	thermal conductivity	$W/(mK)$
-----------	----------------------	----------

Physical size

ΔT	temperature difference	K
------------	------------------------	-----

$\partial T/\partial x$	temperature gradient	K/m
-------------------------	----------------------	-------

U	inner energy	J
-----	--------------	-----

dP	dynamic Price of the electricity	
----	----------------------------------	--

N	length of the predictive horizon	
---	----------------------------------	--

A. Appendix

A.1. Model values

	Start values	Identified values
C_{inside}	400425 J/W	1198069 J/W
C_{envelope}	24999045 J/W	24998057 J/W
C_{interior}	22960754 J/W	22960750 J/W
C_{floor}	26118734 J/W	26118731 J/W
R_{inside}	191 K/W	0,66 K/W
R_{window}	34 K/W	0.0025 K/W
R_{envelope}	287 K/W	0,00008 K/W
R_{interior}	77 K/W	28001 K/W
R_{floor}	749 K/W	2719 K/W
R_{in}	191 K/W	191 K/W
$f_{\text{sol,inside}}$	0,25	7.80685 K/W
$f_{\text{sol,envelope}}$	0,25	-7.30632 K/W

Table A.1. Start and identified values of the model parameters

A.2. Matrices of state-space formulation

$$B_1 = \begin{pmatrix} 1 & 0 \\ 0 & 0 \\ 0 & 0 \\ 0 & 0 \\ -1 & 1 \end{pmatrix} \quad (\text{A.1})$$

A. Appendix

$$B_2 \begin{pmatrix} f_{sun,inside} & 0 & \frac{1}{C_{inside}R_{window}} & 0 \\ 0 & f_{sun,envelope} & \frac{1}{C_{envelope}R_{envelope}} & 0 \\ 0 & 0 & 0 & 0 \\ 0 & 0 & 0 & 0 \\ 0 & 0 & 0 & -1 \end{pmatrix} \quad (A.2)$$

$$C = \begin{pmatrix} 1 & 0 & 0 & 0 & 0 \end{pmatrix} \quad (A.3)$$

A.3. Laboratory journal

Experiment: 16. July - 18. July 2021

Time	Location	Incident
16.7.21 9.30pm	Room 1	HoHe on
	Room 2	HoHeF on
	Floor 2	IH on closed doors
18.7.21 0.00am	Room 2	HoHeF off rearrange HoHeF
	Kitchen	HoHeF on
18.7.21 9.30pm	Room 1	HoHe off
	Kitchen	HoHeF off
	Floor 2	IH off opened doors and windows

Table A.2. Laboratory journal: 16. July - 18. July 2021

Experiment: 16. July - 18. July 2021

A. Appendix

Time	Location	Incident
26.7. - 27.7.21 10.00pm - 5.00am	Kitchen	HoHeF on closed door
27.7. - 28.7.21 10.00pm - 4.00am	Kitchen	HoHeF on closed door
28.7. - 29.7.21 10.00pm - 5.00am 5.00am - 8.20am	Kitchen	HoHeF on opened door closed door
29.7. - 30.7.21 16.00pm - 9.30am	all Kitchen	breakdown PLC HoHeF still off
30.7.21 9.30pm	Room 1 Room 2 Floor 2	HoHe on HoHeF on IH on opened doors
31.7. - 1.8.21 2.30pm - 9.20am	all	breakdown PLC
31.7.21 4.00pm 7.30pm	Room 1 Room 2 Floor 2 Room 2	HoHe off HoHeF off IH off rearrange HoHeF
1.8.21 9.30pm	Room 1 Kitchen	HoHe on HoHeF on PLC works
1.8.21 11.30am - 0.20pm	all	breakdown PLC
1.8.21 9.30pm	Room 1 Kitchen Floor 2	HoHe off HoHeF off IH off opened doors and windows

Table A.3. Laboratory journal: 26. July - 1. August 2021

A.4. Average comfort and grid services

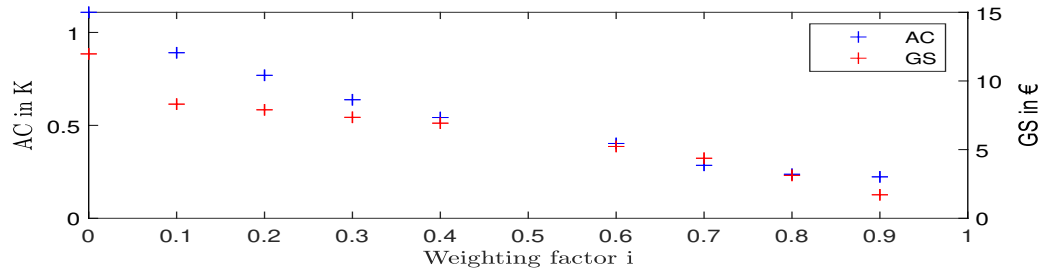


Figure A.1. AC and GS for $N = 12h$

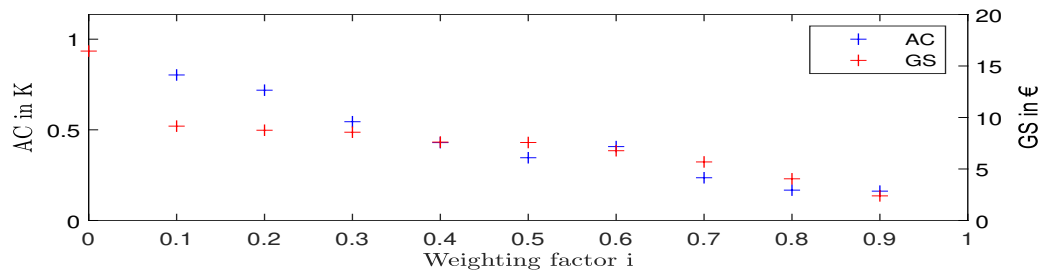


Figure A.2. AC and GS for $N = 18h$

A. Appendix

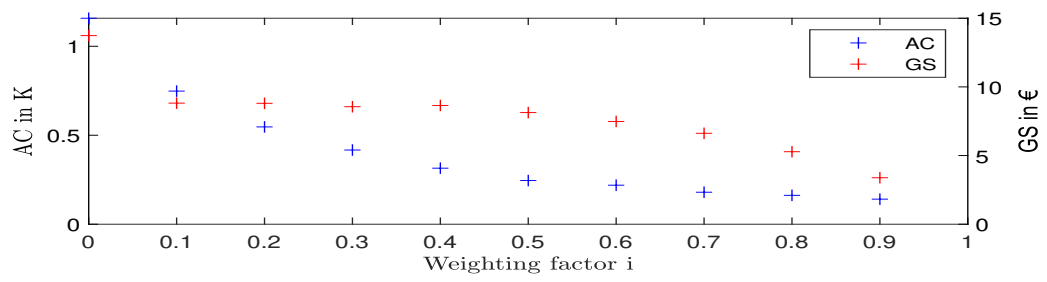


Figure A.3. AC and GS for N = 30h

...